An Influence Model Approach to Failure Cascade Prediction

by

Xinyu Wu

Submitted to the Department of Aeronautics and Astronautics
in partial fulfillment of the requirements for the degree of

Master of Science in Aeronautics and Astronautics

at the

MASSACHUSETTS INSTITUTE OF TECHNOLOGY

September 2020

Author . . . .
Department of Aeronautics and Astronautics
August 2, 2020

Certified by . . . .
Eytan Modiano
Professor, Aeronautics and Astronautics
Thesis Supervisor

Accepted by . . . .
Zoltan Spakovszky
Professor, Aeronautics and Astronautics
Chair, Graduate Program Committee

An Influence Model Approach to Failure Cascade Prediction

by

Xinyu Wu

Submitted to the Department of Aeronautics and Astronautics
on August 2, 2020, in partial fulfillment of the
requirements for the degree of
Master of Science in Aeronautics and Astronautics

Abstract

Power systems are vulnerable to widespread failure cascades which are challenging to model and predict. The ability to predict the failure cascade is important for contingency analysis and corrective control designs to prevent large blackouts. In this thesis, we study an influence model framework to predict failure cascades and try to figure out their underlying pattern in real power systems. A hybrid learning scheme is proposed to train the influence model from simulated failure cascade sample pools. The learning scheme firstly applies a Monte Carlo approach to quickly acquire the pairwise influences in the influence model. Then, a convex quadratic programming formulation is implemented to obtain the weight of each pairwise influence. Finally, an adaptive selection of threshold for each link is proposed to tailor the influence model to better fit different initial contingencies. We test our framework on a number of large scale power networks under both DC and AC flow models, and verify its prediction performance through numerical simulations in both accuracy and efficiency. Under limited training samples, the proposed framework is capable of predicting the final state of links within 10% error rate, and the failure cascade size within 7% error rate in most cases, along with around two magnitude of time cost reduction in large systems compared with flow calculation method. We also show that the trained influence model can unveil instructive insights on cascade properties such as influence sparsity, the relationship between influence value and topological distance of different transmission links, and critical/non-critical initial contingencies.

Thesis Supervisor: Eytan Modiano
Title: Professor, Aeronautics and Astronautics

Acknowledgments

I greatly appreciate the support from Professor Eytan Modiano, and Dr. Dan Wu in this work. Professor Modiano mentored and guided me in formulating and solving a research problem. Dr. Dan Wu, a post-doc in MIT and an expert in power and energy system research, tutored me in the fundamentals of power systems, and we discussed the details of the model, method, and experiments associated with this work. In addition, my work benefited from Professor Ian Dobson from Iowa State University and Professor Paul Hines from University of Vermont. I also want to thank my colleagues in the Communication Network Research Group (CNRG) for their advice and support, both in research and in my life during the past two years. Finally, I want to thank my parents' support from China. This work could not have been done without the help of all of the above people.

Contents

List of Figures

List of Tables

Chapter 1

Introduction

Modern power systems frequently experience unexpected component failures which are caused by falling tree branches, storms, lightening strikes, aged devices, wrong protective actions, etc. These random failures, if not treated properly, can propagate to other system components and eventually lead to enormous blackouts. In Northeast America on Aug. 14, 2003, a 345kV line tripped off after touching a tree limb, which, within one hour, led to expansion of failures from several links to over 500 generating units in the US and Canada [1]. In July 2019, Midtown Manhattan in New York sank into sudden darkness, most likely owing to a disabled transformer [2], and within a month, on Aug. 9, London underwent a similar experience due to the loss of two generators [3].

Past events have shown that large scale blackouts are usually accompanied by a rapid propagation of failures among many system components. This “rolling snowball” phenomenon is referred to as a *failure cascade* in the power system literature. Past failure cascades share some common features. First, they are subject to environments. Several components may be tripped off simultaneously by winds or lightening, which contains combinatorial many possible cases [1–3]. Second, they are subject to man-made decisions, including load shedding and power flow re-dispatch. Such decisions may vary among different systems and operators [4]. Third, the dynamic interaction among hundreds of thousands of components in large scale systems may be highly nonlinear and varying with time [5]. Finally, they do not necessarily propagate locally [6, 7]. Spatially remote components may also fail, rendering the protection over components topologically adjacent to initial contingency insufficient. All these features pose great difficulty in modeling and predicting failure cascades.

Many efforts have been devoted to constructing reasonable models to capture failure cascades. A commonly used failure cascade model attempts to solve the static power flow problem step-by-step to determine the sequence of (quasi) static transmission link overflows that occur before the system finally satisfies all the engineering constraints [6]. In this failure cascade model, solving the AC power flow problem suffers from a heavy computational burden. It is also difficult to find an AC power flow solution when the network configuration changes drastically [5]. Thus, most works applied the simplified DC power flow model in the failure cascade analysis. Although the DC power flow is a linearized version of the AC model, it still requires significant computational efforts when solving it repeatedly in the failure cascade screening process. A few works have been done to derive a closed form solution for the link flows when some links are tripped off [8, 9]. This approach has to take the pseudo-inverse of the system admittance matrix, and has to reformulate the solution when islanding occurs.

In view of the above difficulties on applying power flow models to analyze the cascade process, a number of existing works attempt to ignore the power flow constraints and concentrate on the contagious cascade process in which new failures only happen over adjacent components. It is referred to as the "contagion model" which originates from the percolation model [10–12]. However, these abstract models overlook the nonadjacent correlations among geographically distant failures, and the complete decoupling with power system dynamics renders these models to be rather inaccurate.

1.1 The Influence Model

To capture the nonadjacent failure propagation, Savathiratham *et. al.* proposed the Influence Model (IM) [13]. It is a special graphic model that considers the influence of all the network components on each individual component. It first establishes the pairwise correlation between any two network components, and then summarizes all the pairwise correlations associated with each single component. This aggregated correlation value of each component, which is called the *influence*, is used to determine the state of this component in the failure cascade prediction. The influence model is essentially a Markovian model which is easy to construct and implement for large scale applications. Thus, it is a powerful tool for analyzing and predicting failure cascades in power networks [14–16].

In order to construct the influence model that can be used for power system failure cascade predictions, Hines et.al. applied the Monte Carlo method to learn the influences from historical cascade records [17]. They focused on generating the appropriate distribution of failure cascade sizes that best match existing records, and applying the model to identify critical components. Zhou et.al. further extended the pairwise influences to capture more complex influences for failure size prediction [18].

1.2 Our Contribution

In this thesis, we propose a hybrid learning framework that can be used to train the influence model from either historical data or synthetic data. Then, we apply our trained influence model to predict the failure cascade sequences for a few large scale power system test cases. Numerical simulations show that our model results in relatively accurate prediction under metrics characterizing different facets, with significant time efficiency advantage compared to the flow computation of the power dynamics. The major contributions are summarized below.

- We proposed a hybrid learning framework that can efficiently train the influence model for very large systems. The proposed learning framework integrates Monte Carlo method with quadratic programming, and an adaptive threshold selection scheme to quickly train the model for making valid predictions.

- We applied the influence model to a few large scale power system test cases to predict their failure cascade sequences under both DC and AC cases. The prediction performances are thoroughly evaluated at different levels of granularity: failure size, final state, and failure time prediction. Moreover, we not only evaluate the prediction performance of the whole system for any new cascade sequence, but also assess the prediction over the state of any specific transmission link we are interested in the system. It is the first time that such comprehensive evaluation is investigated on cascade failure prediction in large systems as far as we are concerned.

- We demonstrated that the influence model trained by the hybrid learning framework can unveil valuable insights about cascade properties in the system, including influence sparsity, relationship between influence and physical distance between transmission links, and critical/non-critical initial contingency identification. Such discoveries may pave the way for more efficient management and corrective design on power systems.

In addition, the influence model trained by the hybrid learning framework promises to be meaningful in industrial applications. Firstly, the learning process can be implemented in parallel, suitable for large cascade systems. Secondly, it needs very small portion ($< 5\%$ generally) of cascading sequence samples for training the model among the huge pool of cascade sequences induced by all the possible initial contingencies. Thirdly, it predicts around two orders of magnitude faster than simulation based on power flow calculation, and such gap is even sharper in power systems with large size and under the AC flow setting.

1.3 Related Works

Failure cascades in power systems have been studied extensively over the past decade. Most works are motivated by historical large blackouts. Vaiman et.al. list possible sources of initially tripped links, and further summarize large blackouts that occurred every year from 1984 to 2006 due to different natural disasters [19]. Hines et.al. further discover from cascade records that the blackout size follows the Weibull distribution when the size is small, and power-law distribution when the size is large [17]. These works, originated from the historical records, reveal basic properties of cascades and pave the way for quantitative modeling and analysis.

However, the scarcity of historical cascade records prohibits the researchers from learning the intrinsic factors that determine failure cascade. To tackle this challenge, a number of works utilized power flow models to generate simulated failure cascade sequences for analysis. Zussman et.al. show that the AC flow model is suitable in characterizing real failure cascade, while DC flow model, which is much less complex, may underestimate the ultimate failure size [5, 20]. For simplicity, most works are based on DC power model. Zussman et.al. analytically reveal how failure propagates with multiple tripped links [8,9] based on solving flow equations, while Beinstock and Varma gain insights using mixed-integer linear optimization [21]. Zussman et.al. also formulate a general failure cascade model predicated on DC flow calculation [6].

Another track for cascade analysis is to utilize flow-free models, getting away from flow calculations. Most of these models are probabilistic. First, percolation-based analysis on random graph models has been used to model local cascades whose failure probability depends on neighboring link degree [10, 11, 22]. Moreover, the branching process is a common tool that measures the distribution of the number of outages in a cascade [23, 24], and the random chemistry algorithm, when combined with such distribution, can efficiently estimate the overall blackout risk [25, 26]. In addition, Hines, *et al.* use differential equations to model the cascade process [27] while Zhang, *et al.* do so by mean field theory [28]. Tse, *et al.* try the chemical master equation model to grasp the collective behavior of failure propagation [29] while Qi, *et al.* learn it via the Expectation-Maximization (EM) algorithm [30].

The influence model also has a role in the study of failure cascade process, especially analyzing cascade dynamics and predicting final blackout size. Naeini, *et al.* conduct a series of works about modeling the transition probability between t-wo network states [14–16]. Dobson, *et al.* further propose an efficient Monte-Carlo based method to acquire reasonable estimation for pairwise influence in the system and demonstrate its capability to identify critical components [17, 18].

1.4 Thesis Organization

The rest of the thesis is organized as follows: Chapter 2 introduces the basics of the influence model and its parameters we need to learn. Chapter 3 introduces our hybrid learning framework in detail. Chapter 4 presents the procedure we generate cascade sequences under DC/AC power flow for training the influence model, and the performance evaluation on several power systems under different metrics. Chapter 5 reveals the insights on the property of cascading failures that the trained influence model can reflect.

Chapter 2

Influence Model

The IM is a Markovian model whose dynamics are described by the state variable transitions. In power system failure cascade analysis, the state variable of the IM is typically chosen to be the binary operational state of each transmission link[1], which takes on values of either 0 (failed) or 1 (normal) respectively [23]. Given the i-th link, we use $s_i[t]$ to denote its state at time step t. The collection $s[t] := [s_1[t], \dots, s_M[t]]' \in \{0,1\}^{M\times 1}$ of all the M link state variables represents the *network state* at time t, and we define $s := \{s[t]\}_{t=0}^{T}$ as the state (failure cascade) sequence where T is the termination time of the cascade.

According to the IM [13], the transition of a state variable $s_i[t]$ from the current time t to the next time $t+1$ is described by

$$\tilde{s}_i[t+1] = \sum_{j=1}^{M} d_{ij}\Big(\mathbf{A}_{ji}^{11} s_j[t] + \mathbf{A}_{ji}^{01}(1 - s_j[t])\Big), \tag{2.1}$$

where

$$\mathbf{A}_{ji}^{11} := P\Big(s_i[t+1] = 1 \mid s_j[t] = 1\Big) \tag{2.2}$$

$$\mathbf{A}_{ji}^{01} := P\Big(s_i[t+1] = 1 \mid s_j[t] = 0\Big) \tag{2.3}$$

are the transition probabilities from the state of link j at t to the state of link i at

[1] Other component can also be considered, for example, the generators and transformers.

$t+1$; $\tilde{s}_i[t+1]$ is the estimated value of $s_i[t+1]$, where $\tilde{s}_i[t+1]$ can be interpreted as the expectation of $s_i[t+1]$, provided equation (2.4) which will be introduced soon. We collect all the $\mathbf{A}_{ji}^{11}$'s into an $M \times M$ matrix $\mathbf{A}^{11}$, and similarly $\mathbf{A}_{ji}^{01}$'s to obtain $\mathbf{A}^{01}$. We refer to each of $\mathbf{A}^{11}$ and $\mathbf{A}^{01}$ as the "pairwise influence matrix".

The weight d_{ij} in (2.1) represents the proportional affect from the link pair-(i, j). If we further require

$$d_{ij} \geq 0, \tag{2.4a}$$

$$\textstyle\sum_{j=1}^{M} d_{ij} = 1, \tag{2.4b}$$

then with given link i, d_{ij} can be regarded as a probability mass function for the pairwise influence of any link j on i. We collect all the d_{ij}'s into an $M \times M$ matrix $\mathbf{D}$, referred to as the "weighted influence matrix".

When $\tilde{s}_i[t+1]$ is obtained, the IM assigns 1 to $s_i[t+1]$ with a probability $\tilde{s}_i[t+1]$, and 0 to $s_i[t+1]$ with a probability $1-\tilde{s}_i[t+1]$. This is a randomized mapping from the unit interval $[0, 1]$ to the binary set $\{0, 1\}$

$$\hat{s}_i[t+1] = \begin{cases} 1 & \text{w.p.} \quad \tilde{s}_i[t+1] \\ 0 & \text{w.p.} \quad 1-\tilde{s}_i[t+1] \end{cases}, \tag{2.5}$$

where $\hat{s}_i[t+1]$ is the predicted binary value of $s_i[t+1]$ after the randomized mapping.

This process can yield different prediction results from the same initial contingencies. To make the prediction consistent, we reduce the randomized mapping to a deterministic bisection scheme with a threshold ϵ_i for each link i:

$$\hat{s}_i[t+1] = \begin{cases} 1 & \text{if } \tilde{s}_i[t+1] \geq \epsilon_i \\ 0 & \text{if } \tilde{s}_i[t+1] < \epsilon_i \end{cases}, \tag{2.6}$$

We collect $\hat{s}_i[t]$ in $\hat{s}[t]$ for all the links and refer to it as the prediction of the network state at time t. Then, the time sequence of $\hat{s}[t]$, denoted as $\hat{s}$, is a predicted failure cascade sequence.

An illustrative example of the IM can be found in Fig. 2-1.

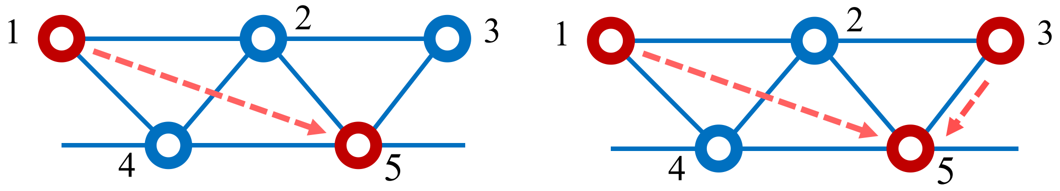

Figure 2-1: We consider a 5-component network and take the influence on component 5 as an example. The left subfigure depicts the pairwise influence of component 1 on 5, concerning $\mathbf{A}_{15}^{11}$ and $\mathbf{A}_{15}^{01}$ in (2.1). The right subfigure reflects that component 5 is mutually influenced by component 1 and 3, where $\mathbf{A}_{15}^{11}$ and $\mathbf{A}_{15}^{01}$ take weight d_{51}, while $\mathbf{A}_{35}^{11}$ and $\mathbf{A}_{35}^{01}$ take weight d_{53} in (2.1).

To apply the IM in failure cascade analysis, the pairwise influence matrices $\{\mathbf{A}^{11}, \mathbf{A}^{01}\}$, the weighted influence matrix $\mathbf{D}$, and the bisection thresholds ϵ_i's need to be specified, which serves as the main theme for the design of the learning mechanism in the following chapter.

Chapter 3

Hybrid Learning Framework for the Influence Model Parameters

In this chapter, we explore how to learn the best values of $\mathbf{A}^{11},\ \mathbf{A}^{01},\ \mathbf{D}$ and ϵ_i's from the set of cascade training samples, denoted as $\mathcal{S}_{train}$. We denote the k-th cascade sequence in $\mathcal{S}_{train}$ as

$$s^k := \{s^k[t]\}_{t=0}^{T_k}, \quad k = 1, 2, \ldots, K,$$

where superscript k is the sample index; K is the total number of training samples; T_k denotes the final time step that the k-th cascade terminates; $s^k[t]$ is the network state at time t; and s^k records the k-th cascade sequence.

Recall (2.1) that $\tilde{s}_i[t+1]$ estimates $s_i[t+1]$ from the IM parameters $\mathbf{A}^{11},\ \mathbf{A}^{01},\ \mathbf{D}$ and the network state $s[t]$ at time t. Hence, the objective is to identify the values of $\mathbf{A}^{11},\ \mathbf{A}^{01},\ \mathbf{D}$ such that the estimation $\tilde{s}_i[t+1]$ can best fit the existing sample $s_i[t+1]$ for every link at all the time steps. We achieve this goal by formulating a constrained optimization problem as follows.

$$\begin{aligned} \min_{\mathbf{D},\mathbf{A}^{11},\mathbf{A}^{01}} \quad & \frac{1}{K}\sum_{k=1}^{K}\sum_{t=1}^{T_k} f(s^k[t], \tilde{s}^k[t]) \\ s.t. \quad & \tilde{s}_i^k[t+1] = \sum_{j=1}^{M} d_{ij}(\mathbf{A}_{ji}^{11} s_j^k[t] + \mathbf{A}_{ji}^{01}(1 - s_j^k[t])), \forall i, k; \\ & \sum_{j=1}^{M} d_{ij} = 1, \forall i; \quad d_{ij}, \mathbf{A}_{ji}^{11}, \mathbf{A}_{ji}^{01} \geq 0, \forall i, j, \end{aligned} \tag{3.1}$$

where $f(s^k[t], \tilde{s}^k[t])$ is the cost function that quantifies the distance between $s^k[t]$ and

$\tilde{s}^k[t]$; M is the number of links.

The problem size of (3.1) is very large because for each link pair (i, j) there exist two independent pairwise influence values $\mathbf{A}^{11}_{ji}$ and $\mathbf{A}^{01}_{ji}$. For example, in a system with $1,000$ links, we have altogether 3×10^6 variables concerning $\{\mathbf{A}^{11}, \mathbf{A}^{01}, \mathbf{D}\}$. In order to improve the computational efficiency, we first train the pairwise influences $\{\mathbf{A}^{11}, \mathbf{A}^{01}\}$ by Monte-Carlo based estimation, and use them to learn the relative influence $\mathbf{D}$ via optimization method, and finally we learn the threshold values ϵ_i for each link i.

3.1 Learning Pairwise Influence Matrices $\mathbf{A}^{11}$ and $\mathbf{A}^{01}$

We apply the Monte Carlo method to learn the pairwise influence matrices $\mathbf{A}^{11}$ and $\mathbf{A}^{01}$ from the sample pool $\mathcal{S}_{train}$ with size K.

Let τ_i^k be the time step that link i changes to failure state in the k-th cascade sequence s^k. If link i does not fail in s^k, we set τ_i^k to be the termination time of s^k. Then, the value of $\mathbf{A}^{11}_{ji}$ for any link i and j is computed by

$$\mathbf{A}^{11}_{ji} := \frac{\sum_{k=1}^{K} C^{11}_{ji}(s^k, \tau_i^k)}{\sum_{k=1}^{K} C^{1}_{j}(s^k, \tau_i^k)} \tag{3.2}$$

where $C^1_j(s^k, \tau_i^k)$ is the number of time steps before τ_i^k in s^k such that link j is normal; $C^{11}_{ji}(s^k, \tau_i^k)$ is the number of time steps before τ_i^k in s^k such that link i is normal, given link j is normal on the adjacent upstream time step.

Similarly, we can estimate $\mathbf{A}^{01}_{ji}$ via

$$\mathbf{A}^{01}_{ji} := \frac{\sum_{k=1}^{K} C^{01}_{ji}(s^k, \tau_i^k)}{\sum_{k=1}^{K} C^{0}_{j}(s^k, \tau_i^k)} \tag{3.3}$$

where $C^0_j(s^k, \tau_i^k)$ is the number of time steps before τ_i^k in s^k such that link j is failed; $C^{01}_{ji}(s^k, \tau_i^k)$ is the number of time steps before τ_i^k in s^k such that link i is normal, given link j is failed on the adjacent upstream time step. In this counting process, we should exclude the samples where link i fails initially because it results from external factors independent of flow dynamics. We also ignore the states of link i after the time step it fails in a sample, as link i will keep failed until termination regardless of network state transitions.

We take the following toy example to gain a more intuitive view of (3.2) and (3.3). We consider two cascade sequences, s^1 and s^2, over 2 links, where

$$s^1 = \begin{bmatrix} 1 & 1 & 1 & 1 & 1 & 0 \\ 1 & 1 & 0 & 0 & 0 & 0 \end{bmatrix}, \quad s^2 = \begin{bmatrix} 1 & 1 & 1 & 0 & 0 & 0 \\ 1 & 1 & 1 & 1 & 1 & 0 \end{bmatrix}.$$

We can observe that $\tau_1^1 = 6$ and $\tau_1^2 = 4$. For $\mathbf{A}_{21}^{11}$, we have $C_2^1(s^1, \tau_1^1) = 2$ and $C_{21}^{11}(s^1, \tau_1^1) = 2$ in s^1, and meanwhile $C_2^1(s^2, \tau_1^2) = 3$ and $C_{21}^{11}(s^2, \tau_1^2) = 2$ in s^2, and similar for $\mathbf{A}_{21}^{01}$. According to (3.2) and (3.3),

$$\mathbf{A}_{21}^{11} = \frac{C_{21}^{11}(s^1, \tau_1^1) + C_{21}^{11}(s^2, \tau_1^2)}{C_2^1(s^1, \tau_1^1) + C_2^1(s^2, \tau_1^2)} = \frac{2+2}{3+2} = \frac{4}{5},$$

$$\mathbf{A}_{21}^{01} = \frac{C_{21}^{01}(s^1, \tau_1^1) + C_{21}^{01}(s^2, \tau_1^2)}{C_2^0(s^1, \tau_1^1) + C_2^0(s^2, \tau_1^2)} = \frac{2+0}{3+0} = \frac{2}{3}.$$

3.2 Learning Weighted Influence Matrix D

Once $\{\mathbf{A}^{11}, \mathbf{A}^{01}\}$ have been obtained, their values can be substituted into (3.1) to form a reduced optimization problem whose decision variables are only from $\mathbf{D}$. We choose the objective function $f(\cdot)$ to be the least square error function, which induces a convex quadratic programming problem as follows.

$$\begin{aligned} \min_{\mathbf{D}} \quad & \frac{1}{K} \sum_{k=1}^{K} \sum_{t=1}^{T_k} \sum_{i=1}^{M} \left(s_i^k[t+1] - \sum_{j=1}^{M} d_{ij} (\mathbf{A}_{ji}^{11} s_j^k[t] + \mathbf{A}_{ji}^{01}(1 - s_j^k[t])) \right)^2 \\ s.t. \quad & \sum_{j=1}^{M} d_{ij} = 1, \forall i; \qquad d_{ij} \geq 0, \forall i, j. \end{aligned} \tag{3.5}$$

The formulation (3.5) can be solved efficiently by numerical methods such as the Frank-Wolfe algorithm [31]. The optimal solution to this problem serves as the Bayes least-squares estimator when $\tilde{s}_i[t+1] = \mathbf{E}[s_i[t+1] \mid s[t]]$. Moreover, the weighted influences on each link i are independent of the influences on any other link j, which further supports a problem decomposition into M sub-problems. We solve these small optimization problems in parallel in practice to further reduce the training time.

3.3 Learning Bisection Threshold ϵ_i

To make a deterministic prediction of a failure cascade, the value of ϵ_i in (2.6) should be provided. A naive way is to set an universal $\epsilon_i = 0.5$ for every link i. However, this undifferentiated threshold value can easily incur wrong predictions. For example in Fig. 3-1, the third row shows that link 2 fails at the fourth time step. However, the fourth row indicates that the predicted state value at the fourth time step is 0.63 which is greater than 0.5. Thus, by (2.6) the state of link 2 will be assigned to 1 instead of 0, misidentifying the failure. Therefore, the threshold value ϵ_i should be selected adaptively according to differential initial contingencies.

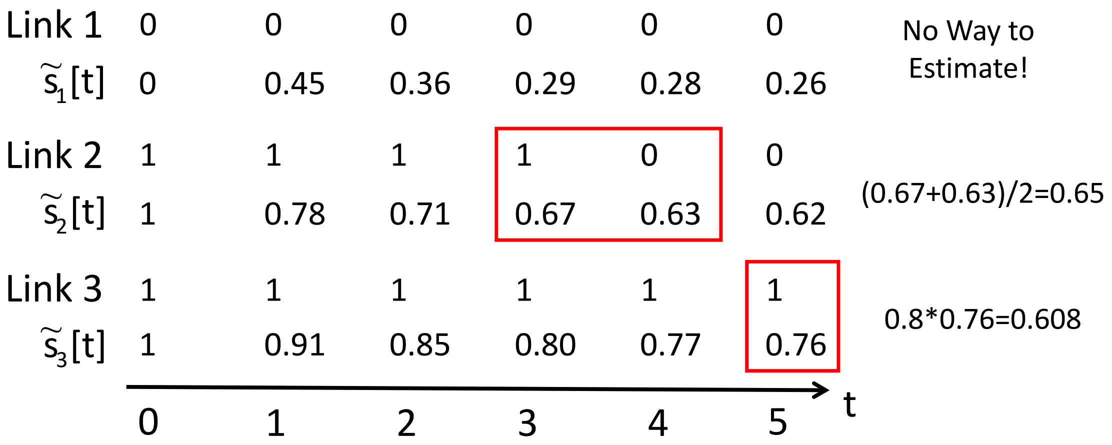

Link 1	0	0	0	0	0	0	No Way to Estimate!
$\tilde{s}_1[t]$	0	0.45	0.36	0.29	0.28	0.26	
Link 2	1	1	1	1	0	0	
$\tilde{s}_2[t]$	1	0.78	0.71	0.67	0.63	0.62	(0.67+0.63)/2=0.65
Link 3	1	1	1	1	1	1	
$\tilde{s}_3[t]$	1	0.91	0.85	0.80	0.77	0.76	0.8*0.76=0.608
	0	1	2	3	4	5	t

Figure 3-1: This is an example of determining thresholds on all 3 link categories in a cascade sample. Each link representative has two rows of records: the first row denotes the real state value at each time step, while the second row denotes the iterative values of $\tilde{s}_i[t]$ for every link i based on (2.1). For link 2 we set ϵ_2^k as the average of $\tilde{s}_2[4]$ and $\tilde{s}_2[5]$, while for link 3 we set ϵ_3^k to be $0.8 \times \tilde{s}_3[T_k] = 0.8 \times 0.76 = 0.608$, where 0.8 can be replaced by any real value within $(0, 1)$.

We summarize our adaptive threshold selection scheme for a specific link i as follows.

1. **Identifying a threshold value of link i in a sample sequence s^k.** Three situations can happen. 1) Link i fails initially in the sample sequence s^k. In this situation, there is no way to know the threshold value. 2) Link i fails but not from the beginning of the sample sequence s^k. Then, we recursively compute the estimated state variable $\tilde{s}_i^k[t+1]$ by assigning $\tilde{s}_j^k[t]$ to $s_j^k[t]$ on the right hand side of (2.1). The critical time step where link i fails is determined. We choose the threshold value for this sequence to be the intermediate value of the estimated state at the critical time step and the estimated state at its upstream adjacent time step. 3) Link i never fails in the sample sequence s^k. In this situation, we recursively compute the estimated state variable $\tilde{s}_i^k[t]$, and choose the threshold value to be $\alpha \times \tilde{s}_i^k[T_k]$ at the final time T_k, where $\alpha \in (0,1)$ can be selected arbitrarily. Fig. 3-1 shows the identification of ϵ_i among these three situations by a toy example.

2. **Forming the threshold pool of link i from all sample sequences.** For each link i, we compute the threshold value ϵ_i^k for every sample sequence s^k and collect them in a set Ω_i, thus forming a K-dimensional vector for each link.

3. **Selecting an appropriate threshold value of link i for a new contingency.** The basic idea is to select the threshold value ϵ_i from the known threshold set Ω_i such that the associated known contingency is "closest" to the new contingency denoted as $s^{new}[0]$. The closest known contingency to $s^{new}[0]$ is defined by[1]

$$k^\star = \arg\min_{k=1,2,\cdots,K} ||s^{new}[0] - s^k[0]||_1 \tag{3.6}$$

   where k is the index of the known contingency; $s^k[0]$ is the known contingency; $s^{new}[0]$ is the new contingency; and $||s^{new}[0] - s^k[0]||_1$ is the L_1-norm, denoting the number of links that have different initial states in $s^{new}[0]$ and $s^k[0]$. Then,

[1] Other ways to select the closest contingency are also possible.

we select the threshold value $\hat{\epsilon}_i$ to be

$$\hat{\epsilon}_i = \epsilon_i^{k^\star}. \tag{3.7}$$

Sometimes multiple solutions for $k^\star$ exist for (3.6). We choose $\hat{\epsilon}_i$ to be the median value among multiple options.

$$\hat{\epsilon}_i = \text{median}\{\epsilon_i^k\}_{k \in K^*} \tag{3.8}$$

where $K^\star$ is the optimal solution set of (3.6). We take median rather than average, as average is subject to anomalous thresholds seriously while median is not.

Through the above steps, we can obtain a bisection threshold estimation $\{\hat{\epsilon}_i\}_{i=1}^M$ for each new initial outages. With all parameters learned, we can now step into cascade prediction.

3.4 Overall Procedure

The overall procedure of learning the IM and using it for failure cascade predictions is presented in Algorithm 1. In the learning modular, finding the weighted influence matrix $\mathbf{D}$ is the most computationally expensive part because it requires solving a convex quadratic programming problem. After that, the remaining computational efforts are much less demanding. The prediction modular in Algorithm 1 is computationally inexpensive since it only requires multiplication and addition manipulations. Therefore, using the IM to predict failure cascades is potentially much faster than using flow equations to make predictions, where computing flows in DC systems needs to solve linear equations multiple times taking $O(n^3)$ time complexity, while that in AC systems costs even more. This claim will be numerically verified later in the performance evaluations in the next chapter.

Algorithm 1: Learning Approach and Failure Cascade Prediction based on Influence Model

```
Input: Training Sample Pool $\mathcal{S}_{train} = \{s^k[t]\}_{t=0,\dots,T_k}^{k=1,\dots,K}$; New Initial State $s^{new}[0]$.
Output: Weighted Influence Matrix $\mathbf{D}$; Pairwise Influence Matrices
        $\{\mathbf{A}^{11}, \mathbf{A}^{01}\}$; Sequence Prediction $\hat{s}^{new}$.
// Learning Influence Model Parameters
Estimate $\mathbf{A}^{11}$ and $\mathbf{A}^{01}$ based on Monte-Carlo Method;
Learn $\mathbf{D}$ from the quadratic optimization (3.5);
Build the threshold set $\Omega_i$ for each link $i$;
Find $k^\star$ based on equation (3.6) and form the set $K^\star$ containing all $k^*$s;
Obtain $\hat{\epsilon}_i$ by equation (3.8) for each link $i$;
// Failure Cascade Prediction
$t \leftarrow 0$;
while there are new links predicted failed at time $t$ do
    $\tilde{s}_i^{new}[t+1] \leftarrow \sum_{j=1}^{M} d_{ij}(\mathbf{A}_{ji}^{11} s_j^{new}[t] + \mathbf{A}_{ji}^{01}(1 - s_j^{new}[t]))$ for each link $i$;
    $\hat{s}_i^{new}[t+1] \leftarrow 0$ if $\tilde{s}_i^{new}[t+1] < \hat{\epsilon}_i$, $\hat{s}_i^{new}[t+1] \leftarrow 1$ otherwise;
    $s^{new}[t+1] \leftarrow \tilde{s}^{new}[t+1]$, $t \leftarrow t+1$;
$T \leftarrow t - 1$;
return $\mathbf{D}$, $\mathbf{A}^{11}$, $\mathbf{A}^{01}$, $\hat{s}^{new}$.
```

Chapter 4

Performance Evaluation

In this section, we present the main evaluation results for failure cascade prediction. Before that we introduce how we generate cascade failure training samples and the power systems we test on, and then we the list performance metrics and methods for comparison.

4.1 Generating Sample Cascade Sequences

The IM parameters $\mathbf{A}^{11}$, $\mathbf{A}^{01}$, $\mathbf{D}$ and ϵ_i's are learned from known failure cascade data. However, the historical failure data of a real power grid is usually inaccessible because the power grid is a critical infrastructure whose data should be kept confidential, and because in a particular power grid large scale failure cascades rarely happen. To get enough data for training the IM, we generate synthetic failure cascades by the power flow based simulation approach [17]. Specifically in this thesis, we solve the DC/AC power flow problem using the MATPOWER Toolbox [32]. The procedures of generating synthetic failure cascades are summarized as follows.

1. Given the loading condition, compute the initial link flows.

2. Randomly initiate an $M-k$ contingency (k initially failed links), where $k=2$ or 3 in our setting.

3. Detect all the islands (disconnected sub-graphs) that appear. If the whole network is connected, then it can be viewed as the only island.

4. Specify a new bus that is connected to the ground in each island.

    - In our setting we specify the bus with lowest loading to be the one connected to the ground.

5. Re-balance the power in each island by either generation curtailment or load shedding depending on whether the supply exceeds the demand.

6. Recompute the link flows in each island.

7. Detect the newly overflowed links, remove the overflowed links and return to Step 3. Otherwise, terminate.

Repeating this procedure we can build up the training sample pool $\mathcal{S}_{train}$. We will use this sample pool to train our IM parameters.

4.2 Dataset Information and Generation

We apply the standard datasets in Matlab MATPOWER toolbox [32]. We choose four systems: 118-bus, 1354-bus, 2383-bus, and 3012-bus power system. The 118-bus system represents small systems. In this case, link capacity information is not provided. We set the capacity of each link to be a certain portion of its flow value, which is greater than 100%, based on the default power injection and loading provided in the dataset. Such portion is termed as the 'Factor of Safety' (FoS). We vary the FoS values to set the capacity values, where lower FoS implies lower capacity values and thus lower robustness. The other 3 power systems are large scale systems with only few link capacity values not given[1], hence we generally use the provided capacity values. For links lacking of capacity information, we set capacity values to be large

[1] The `rateA` in each system data in MATPOWER toolbox denotes the given capacity values [32].

enough such that they are free from failure during the cascade process. These two different settings of link capacity values can also show that the prediction framework based on influence model can be applied to broader settings.

We consider both DC and AC power flow models. The generation of cascade sequences has been shown in the last section. Here we supplement more details:

- For DC case, the power flow on a link (i, j) is exactly the active power, denoted as P_{ij}, and thus the flow $f_{ij} = P_{ij}$. For AC case, the power flow on a link (i, j) contains both active power P_{ij} and reactive power Q_{ij}, and from the dataset we find $P_{ij} \neq P_{ji}$ and $Q_{ij} \neq Q_{ji}$, hence we refer to [5] to calculates the power flow f_{ij} as
$$f_{ij} = \frac{1}{2}(\sqrt{P_{ij}^2 + Q_{ij}^2} + \sqrt{P_{ji}^2 + Q_{ji}^2}).$$
- We use Newton-Raphson method [33] to solve nonlinear equations in AC power model in each island during cascade. However sometimes it does not converge. In this case, we should do load shedding. Specifically, we proportionally decrease the power injection and loading until convergence [5]. In our setting, we decrease 20% power and loading in every trial of calculation before convergence, and shed all power and loading to be 0 in the corresponding island after 10 unconverged trials to avoid unnecessary time waste.

Under both DC and AC models, we consider at most 50000 cascade sequence samples for training in each system, and will vary the size of training set. We focus on $M - 3$ initial contingencies in 118-bus system due to its small size, while $M - 2$ initial contingencies in larger systems such that the ratio of training samples we use matches to that in 118-bus systems generally, where $M - k$ denotes k links fail initially among all M links in the system. Note that the ratio of the training samples compared with the set of all possible $M - k$ initial contingencies is very low, for example in 1354-bus system, the ratio is $50,000/\binom{1710}{2} = 3.4\%$, and such ratio is even lower in other cases.

In addition, we observe that in each network system, there exist some transmission links that have never experienced failure induced by the cascade process initiated by the outages of other links. Such links do not provide any information about their failures, hence we exclude them and term the rest as *effective links* which we consider in performance evaluation.

Note that there are many possible settings in each system, including different power injection, loading, and capacity values. Therefore for convenience, we define a *default setting* for each system. We set FoS= 1.2 as the default setting for 118-bus system, and set the loading and capacities provided in MATPOWER toolbox for the other 3 systems as their corresponding default settings. Table 4.1 presents the information for cascade samples in 4 systems under DC model and their default settings, while Table 4.2 presents that under AC model, where *#Eff. Rate* is the portion of effective links in the system, and *Fail Size* is the total number of link outages in a cascade sequence sample. The data is calculated from $50,000$ cascade samples induced by different initial contingencies. We can find that the failure size varies in a wide range, thus nontrivial to predict the cascade sequences induced by different initial contingencies.

Table 4.1: Default Sample Information under DC

System	118-Bus	1354-Bus	2383-Bus	3012-Bus
#Generators	54	260	327	297
#Links	179	1710	2886	3566
#Eff. Links	171	762	2088	2083
Eff. Rate	95.5%	44.6%	72.4%	58.4%
Avg. Fail Size	98	179	598	263
Max Fail Size	140	314	862	792
Min Fail Size	3	2	110	11

Table 4.2: Default Sample Information under AC

System	118-Bus	1354-Bus	2383-Bus
#Generators	54	260	327
#Links	179	1710	2886
#Eff. Links	177	1547	2815
Eff. Rate	98.9%	90.5%	97.5%
Avg. Fail Size	109	80.3	390
Max Fail Size	160	1292	2606
Min Fail Size	3	2	2

4.3 Performance Metrics

To evaluate prediction performance, we consider two sets of metrics.

- **Sample-based metrics**: This set of metrics captures the prediction performance for each cascade sequence samples in the test set. Acceptable performance on these metrics shows the applicability to well predicting the cascade sequence caused by any set of initial contingencies in general.

- **Link-based metrics**: This set of metrics captures the prediction performance on each link among all the cascade sequences in the test set. Acceptable performance on these metrics shows the accuracy of the prediction mechanism on the link we target at, for example such bottleneck links in the system, which can not be fully captured by the sampled-based metrics.

4.3.1 Sample-based metrics

Sample-based metrics include:

- **Avg. Failure Size Error Rate** l_{size}: $l_{size} = \frac{1}{K}\sum_{k=1}^{K} l_{size}^{k}$, where l_{size}^{k} is the failure size prediction error, relative to real failure size, in the k-th test sample.

- **Avg. Failure Frequency Error** l_{freq}: $l_{freq} = \frac{1}{M}\sum_{i=1}^{M} l_{freq}^{i}$, where l_{freq}^{i} is the absolute difference between real and predicted failure frequency of link i among all test samples.

- **Avg. Final State Error Rate** l_f: $l_f = \frac{1}{K}\sum_{k=1}^{K} l_f^k$, where l_f^k is the ratio of links whose final states are mistakenly predicted, in the k-th test sample.

- **Avg. Failure Time Error** l_t: $l_t = \frac{1}{K}\sum_{k=1}^{K} l_t^k$, where l_t^k is the failure time prediction error among all links that fail eventually in the k-th test sample.

Fig. 4-1 and Fig. 4-2 illustrates the way we calculate l_{size}^{k}, l_{freq}^{i}, l_f^k, and l_t^k for each test sample s_{test}^{k} and each link i. For l_{size}^{k}, l_{freq}^{i}, and l_f^k, we use Venn graph, divided into four disjoint subsets A, B, C, D, to show the calculation. Inside, $A \cup C$ denotes the set of real failures, $B \cup C$ denotes the set of predicted failures, C is the set of correctly predicted failures, while D represents links not failed and meanwhile not predicted to be failed, under each metric.

- For l^k_{size}, $|A^k_{size} \cup C^k_{size}|$ is the real failure size while $|B^k_{size} \cup C^k_{size}|$ is the predicted failure size in s^k_{test}, and

$$l^k_{size} = \frac{\Big| |B^k_{size} \cup C^k_{size}| - |A^k_{size} \cup C^k_{size}| \Big|}{|A^k_{size} \cup C^k_{size}|} \times 100\%.$$

- For l^i_{freq}, $|A^i_{freq} \cup C^i_{freq}|$ is the total number of test samples in which link i fails but not from the beginning, while $|B^i_{freq} \cup C^i_{freq}|$ is our prediction towards it, and

$$l^i_{freq} = \Big| |B^i_{freq} \cup C^i_{freq}| - |A^i_{freq} \cup C^i_{freq}| \Big|.$$

- For l^k_f, $|A^k_f \cup B^k_f|$ is the number of links whose final states we mistakenly predict in s^k_{test}, while $|A^k_f \cup B^k_f \cup C^k_f \cup D^k_f|$ denotes the number of effective links, and

$$l^k_f = \frac{|A^k_f \cup B^k_f|}{|A^k_f \cup B^k_f \cup C^k_f \cup D^k_f|} \times 100\%.$$

For l^k_t, we take an example on a cascade sequence over 6 links that fail during the cascade. Each number in the first row denotes the time step a link changes to failure, while each number in the second row denotes our prediction on the time step[2]. We ignore counting in initially failed links in all the 4 metrics.

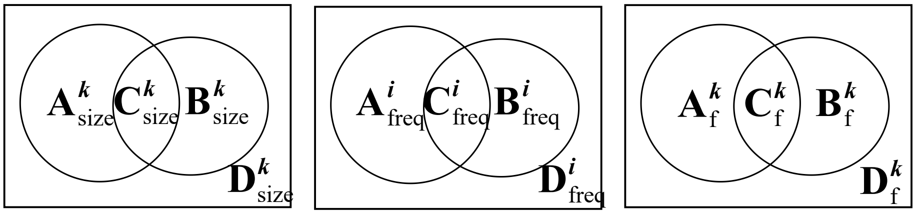

Figure 4-1: An illustrative example of l_{size}, l_{freq}, l_f

These metrics represent four levels of granularity shown in Fig. 4-3. l_{size} focuses on the number of failures but does not care about the accuracy on each link. l_{freq} casts light on failure risk of each link, but does not specify in which case a link will

[2] If we predict a link to be normal, then the corresponding number in the second row is our predicted termination time of this cascade.

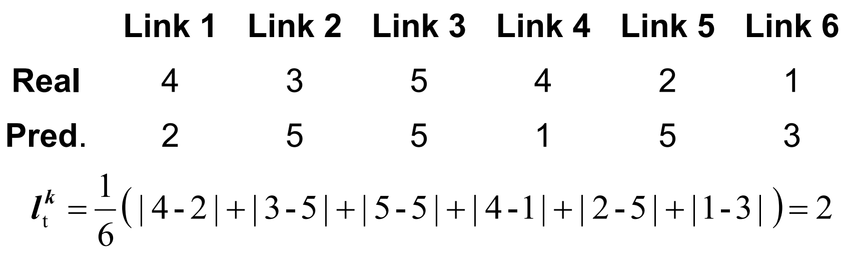

	Link 1	Link 2	Link 3	Link 4	Link 5	Link 6
Real	4	3	5	4	2	1
Pred.	2	5	5	1	5	3

$$l_t^k = \frac{1}{6}\left(|4-2|+|3-5|+|5-5|+|4-1|+|2-5|+|1-3|\right)=2$$

Figure 4-2: An illustrative example of l_t

fail. l_f reflects the binary prediction accuracy on each link in each cascade, while l_t further unveils the prediction performance at each time step. To the best of our knowledge, this is the first attempt to evaluate these four levels of metrics.

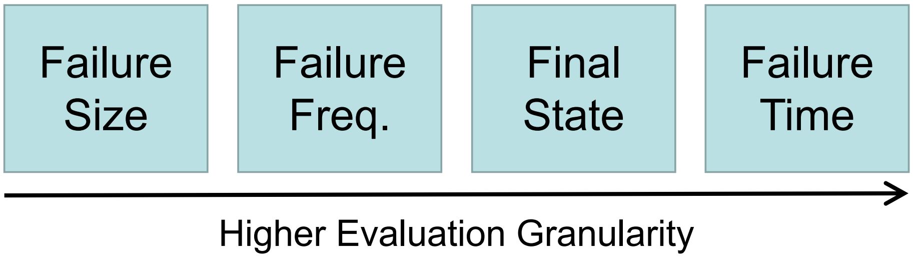

Figure 4-3: Four levels of granularity in performance evaluation

4.3.2 Link-based metrics

We consider the following four link-based metrics. We use an example to explain these metrics. We focus on a specific link i, and its final state in 8 different cascade sequences is respectively $[0, 1, 1, 0, 0, 1, 0, 1]$, in which link i fails initially in the 4th sample.

- **Link i Final State Prediction Error Rate $l_{f,i}$:** $l_{f,i}$ denotes the ratio of corrected final state prediction for link i among all test samples except for cases that link i trips initially. In the example, if we predict its final states to be $[1, 1, 0, 0, 0, 0, 1, 0]$, then $l_{f,i} = 4/7 \approx 57\%$.

- **Link i Final State Miss Detection Rate $l_{md,i}$:** $l_{md,i}$ denotes the ratio of predicting link i to be normal among all test samples that link i fails, except for cases that link i trips initially. It reflects the ratio of failure misidentification. In the example, if we predict its final states to be $[1, 1, 0, 0, 0, 0, 1, 0]$, $l_{md,i} = 2/3 \approx 67\%$.

- **Link i Final State False Alarm Rate** $l_{fa,i}$: $l_{fa,i}$ denotes the ratio of predicting link i to be failed among all test samples that link i is normal during the cascade process except for cases that link i trips initially. In the above example, if we predict its final states to be $[1, 1, 0, 0, 0, 0, 1, 0]$, $l_{fa,i} = 3/4 = 75\%$.

- **Link i Time Prediction Error** $l_{t,i}$: $l_{t,i}$ denotes the average failure time prediction error for link i among all test samples that link i fails except for cases that link i trips initially. Suppose in the above example, the failure time record of link i is $[2, 7, 8, 1, 5, 7, 4, 6]$ and our prediction is $[3, 5, 9, 1, 4, 2, 7, 6]$, then $l_{t,i} = \frac{1}{3}(|2-3| + |5-4| + |4-7|) \approx 1.67$, as link i fails during the cascade process only in the 1st, 5th, and 7th sample.

Compared with the sample-based metrics, link-based metrics capture the different prediction difficulties among different links. For example, if a link i fails in 5% of all test samples, then it is trivial to achieve $l_{f,i}$ to be 5% by always regarding i to be normal, hence for this link, our prediction is valid only if $l_{f,i} < 5\%$ by our method. In addition, to achieve low $l_{md,i}$ is hard for such a link, as within 100 test samples, if in 5 of them link i fails, and there is only one misidentified failure of i, then $l_{md,i} = 20\%$. In the opposite, if for link i, its failure frequency is very high, then to achieve low $l_{fa,i}$ is hard. Moreover, link i which fails at frequency 50% will lead to the largest $l_{f,i}$ under the trivial prediction. Therefore, we should evaluate the prediction performance on each link based on their failure frequency.

4.4 Performance Evaluation on DC systems

In this part, we present the evaluation results for failure cascade prediction over 4 power systems under DC flow model. In each system, we test on 3 different cases by varying the capacities values or loading levels, and evaluate both sample-based and link-based metrics.

4.4.1 Sample-based metrics

We summarize our main results for failure cascade prediction in order of granularity. For 118-bus system, we proportionally increase the capacity value of all the links while keeping the power generation and loading invariant, and induce FoS to be 1.2, 1.5 and 1.8. For larger systems, we proportionally increase power generation and loading to study the performance under different loading conditions. In the 1354-bus system, we take 1×, 1.5× and 2× of its original power injection and loading, while in the 2383-bus and the 3012-bus system we take 1×, 1.25×, and 1.5×, where the lower power injection and loading level increment in ratio than that in 1354-bus system is because the default settings for these two systems are measured at peak power in winter.

Under all the settings, we evaluate the prediction performance on $2,000$ test samples, different from any training sequence in $\mathcal{S}_{train}$. For each metric, we present two categories of results. The first is how the performance varies from $5,000$ to $50,000$ training samples. The second is the cumulative distribution function (CDF) of the corresponding error metric on each test sample with $50,000$ training samples.

Level 1–Failure Size l_{size}: Fig. 4-4 shows the results on l_{size}. The column on the left captures the value of l_{size} under more training samples. Generally, by incorporating more training samples, l_{size} becomes lower and drops below 7%. For example, if 200 links fail eventually, then our predicted failure size will be within $[186, 214]$ on average. Besides, the decreasing trend of l_{size} is obvious before $20,000$ in most cases, and then diminishes after that, indicating that our approach can offer good enough failure size prediction with limited cascade records in these cases. The column on the right shows the CDF plots. We can find that in each case, l_{size} is less than 10% in more than 85% of test samples, and almost all predictions will not make l_{size} larger than 30%.

Level 2–Failure Frequency l_{freq} Fig. 4-5 presents the results on l_{freq}. Gen-

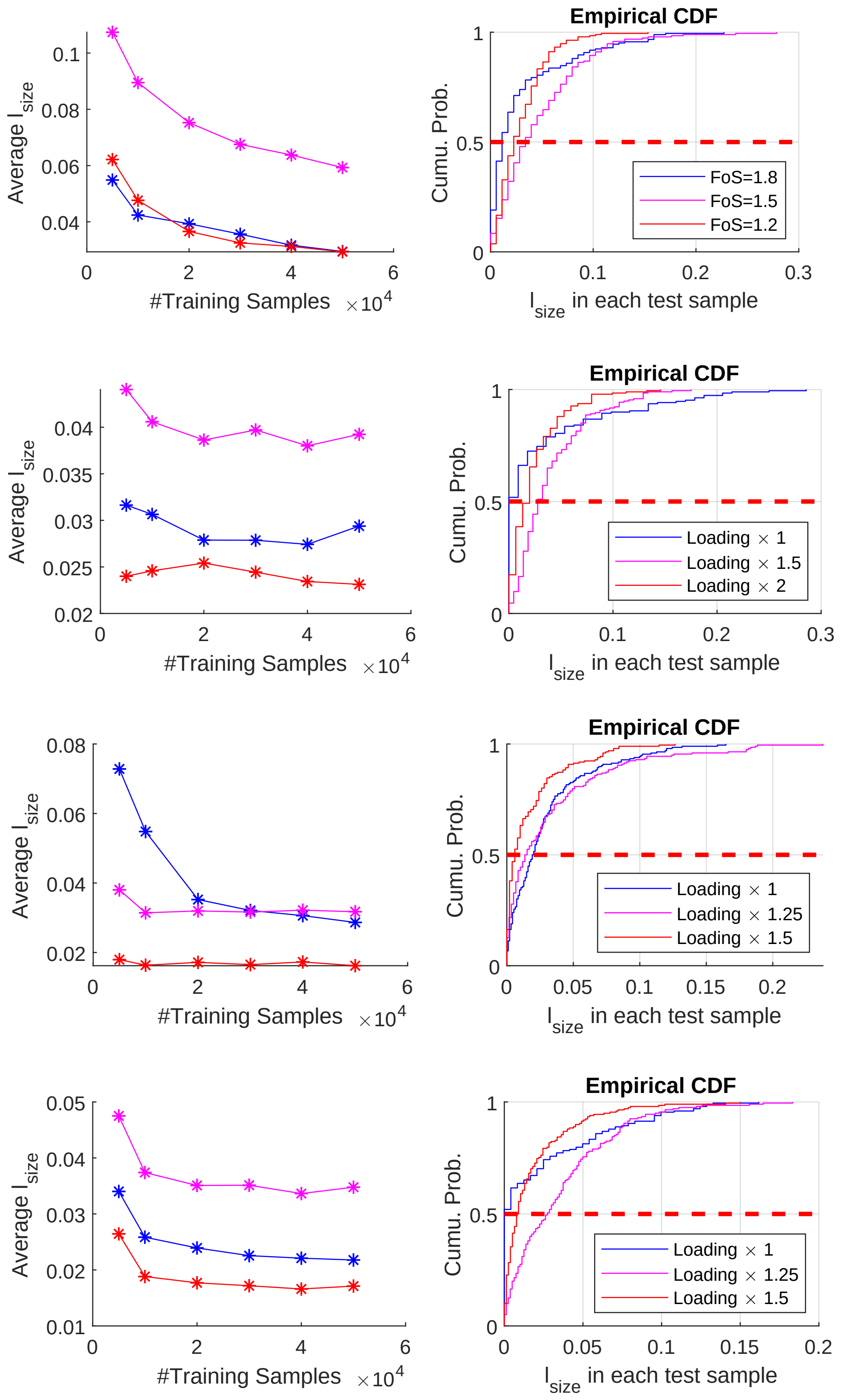

Figure 4-4: Results on l_{size}: 118, 1354, 2383, 3012-bus systems in order

erally, $l_{freq} \leq 0.08$ in almost all cases, which indicates that the absolute frequency prediction error will not deviate much. For example, if a link fails with frequency 0.3, then our prediction on it will lie within $[0.22, 0.38]$ in expectation. Unlike l_{size}, however, l_{freq} does not decrease monotonically in our simulations. Fig. 4-5 shows some fluctuations of l_{freq} when we tested on different sample sets. It may require more sample data to stabilize. From the CDF plots, we can observe that under most conditions around 75% of the links have $l_{freq} < 0.1$. However, the medium loading conditions in 1354-bus and 3012-bus systems yield the worst CDF results. It is caused by the fact that a light loading condition or a heavy loading condition induces a rather simple failure cascade situation (either mostly in small scale or mostly in large scale), however, a medium loading can introduce a more complicated failure cascade situation, sometimes in small scale and sometimes in large scale.

Level 3–Final State l_f: Fig. 4-6 presents the results on l_f. We can observe that l_f declines generally as more training samples are involved, and l_f can be lower than 10% in most cases. This means that among $1,000$ effective links, we can predict more than 900 of them correctly in average under different initial outages. The CDF plots further demonstrate that for at least half of the test samples, l_f will be smaller than 10% among all tested conditions, and altogether more than 95% of all the predictions cause l_f smaller than 30%.

Level 4–Failure Time l_t: Fig. 4-7 illustrates the results on l_t. l_t mostly decreases under more training samples, while in other settings the error keeps stable at a low level. In most of cases, l_t is within 1 time step, showing that failure time prediction is valid. For example, in 1354-bus system the cascade generally lasts for 10 time steps, if it lasts for 20 minutes in reality, then our prediction can cause error within 2 minutes in most situations. In perspective of CDF, we can further draw that in most cases, around 90% of test samples can achieve time error within 2 steps, while larger l_t generally appears in medium loading conditions. This may stem from longer cascade duration under medium loading, i.e., more time steps before the cascade terminates, since under high loading the failure propagates rapidly and terminates in few steps, while under low loading it also stops early due to the limited failure size.

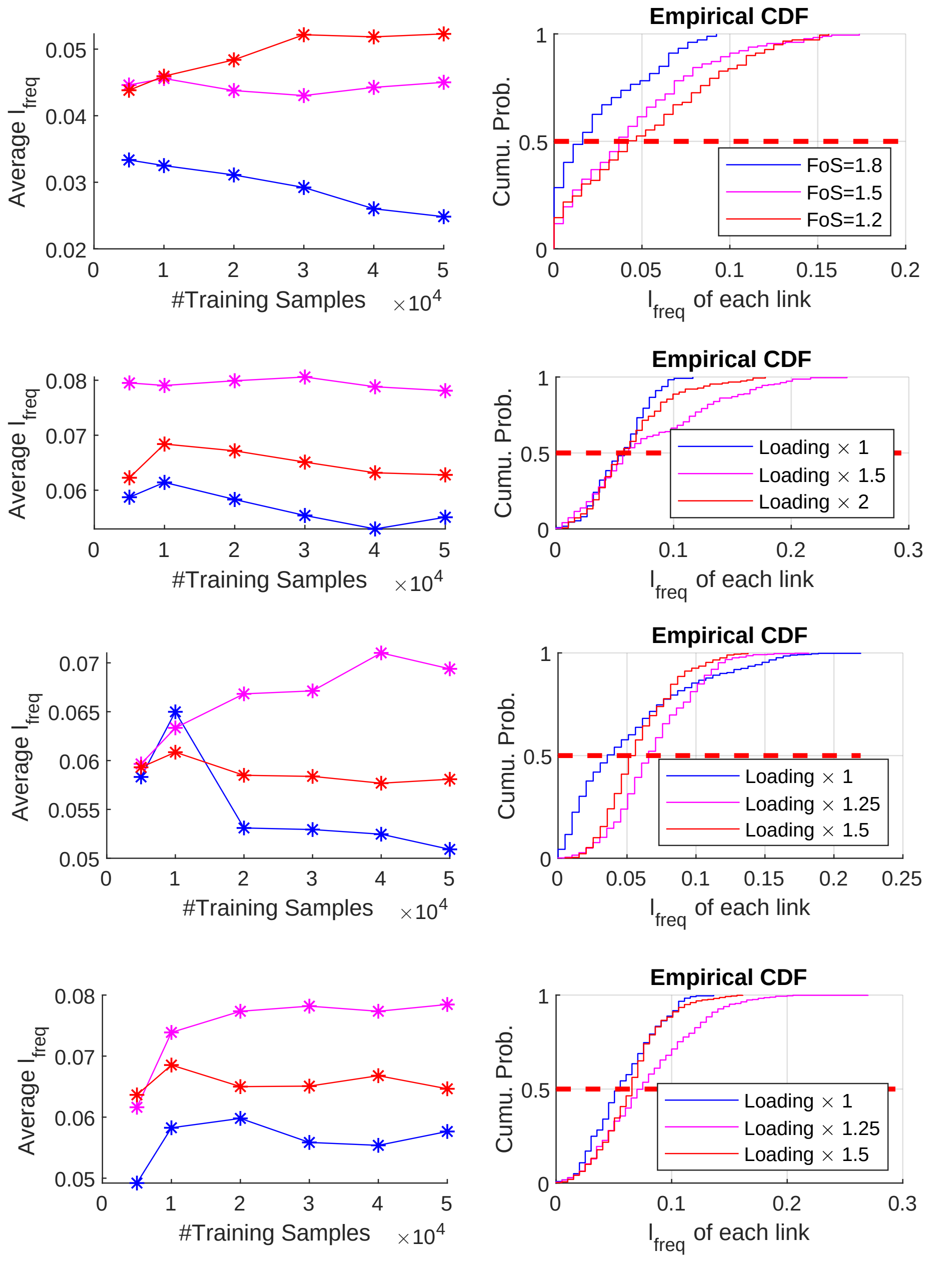

Figure 4-5: Results on l_{freq}: 118, 1353, 2383, 3012-bus systems in order

In addition, note that in the metrics l_{size}, l_f and l_t, the decreasing trend of the metrics is not strict. This is because the training samples we gather only accounts for very limited amount, hence there might exist deviations and fluctuations. However, the general decreasing trend has evinced the validity of prediction based on learning the influence model.

4.4.2 Link-based metrics

In this part, we focus on the four link-based metrics. In the evaluation, we classify all the links in the systems into 10 groups based on their frequency of experiencing failure caused by the cascade among all the training samples. The groups include failure frequency intervals: $[0\%, 10\%), [10\%, 20\%), \ldots, [90\%, 100\%)$. For example, among all $10,000$ cascade samples, if link i fails $1,202$ times while it fails at the beginning before cascade starts for 2 times, then its failure frequency is calculated as $(1202-2)/10000 = 12\%$, hence belonging to the frequency interval $[10\%, 20\%)$. We will evaluate the prediction performance on each group of links, as we have mentioned earlier that different link groups turn in different prediction difficulties under different metrics.

Fig. 4-8, 4-9, 4-10 and 4-11 present the results on link-based metrics over the four systems under DC flow model. We only present one loading condition for each system, where FoS$= 1.8$ for 118-bus case, $2\times$ default loading for 1354-bus case, and $1.5\times$ default loading for 2383-bus and 3012-bus cases. Other loading conditions lead to results with similar pattern. For each system, the four subfigures represent the evaluation on $l_{f,i}$, $l_{md,i}$, $l_{fa,i}$ and $l_{t,i}$ in order. For all the metrics, we calculate the average metric value among all the links in each failure frequency interval, marked as asterisks in each subfigure.

In our experiment we calculate the failure frequency of each link based on the 50,000 training cascade samples, and we evaluate the prediction using 5,000; 10,000; 30,000; and 50,000 of them. Besides, to show that our prediction mechanism literally works, we compare it with two trivial prediction methods: deterministic trivial prediction and randomized trivial prediction. Deterministic trivial prediction is to always predict a link to be failed if its failure frequency is larger than 50%, and to

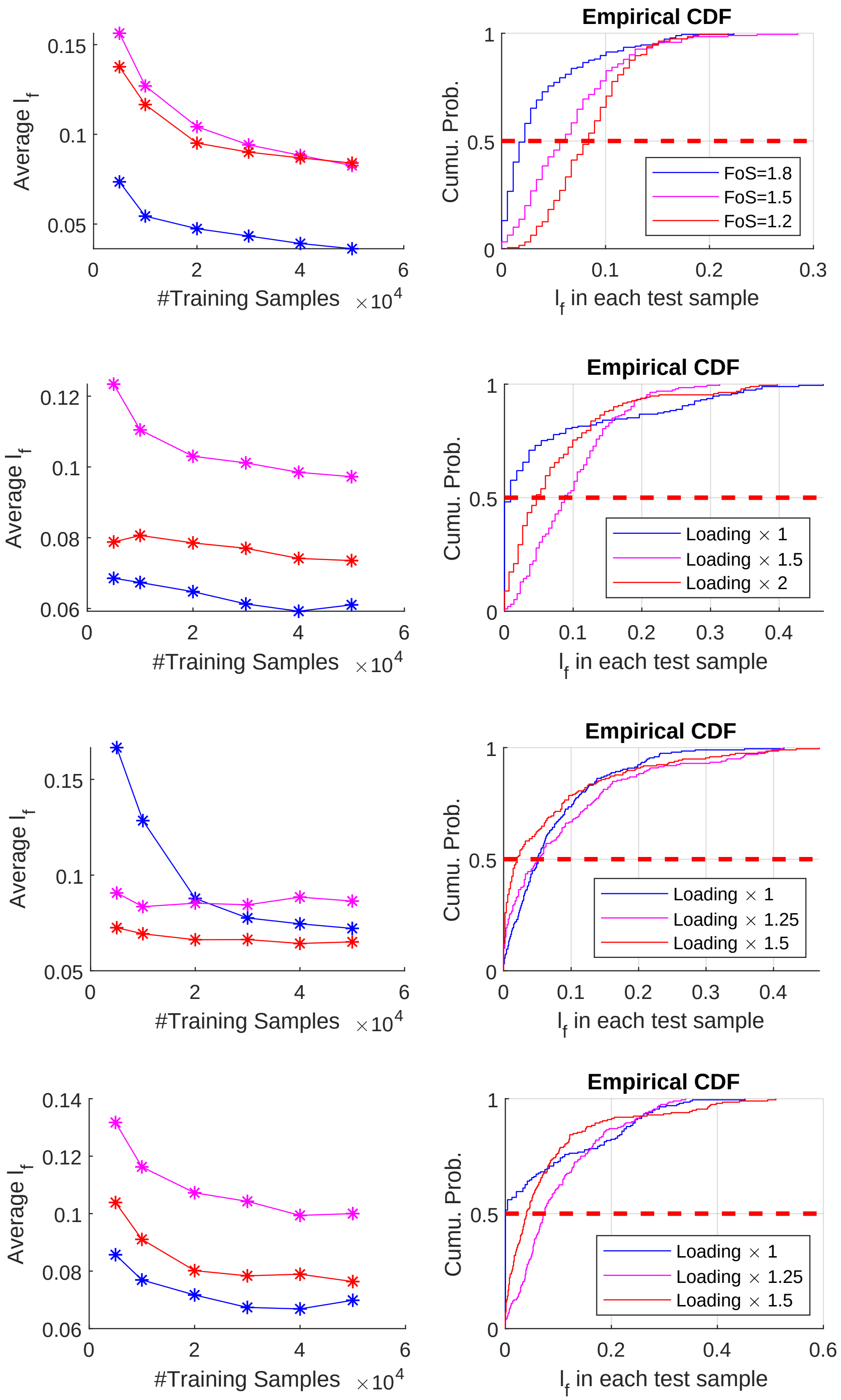

Figure 4-6: Results on l_f: 118, 1354, 2383, 3012-bus systems in order

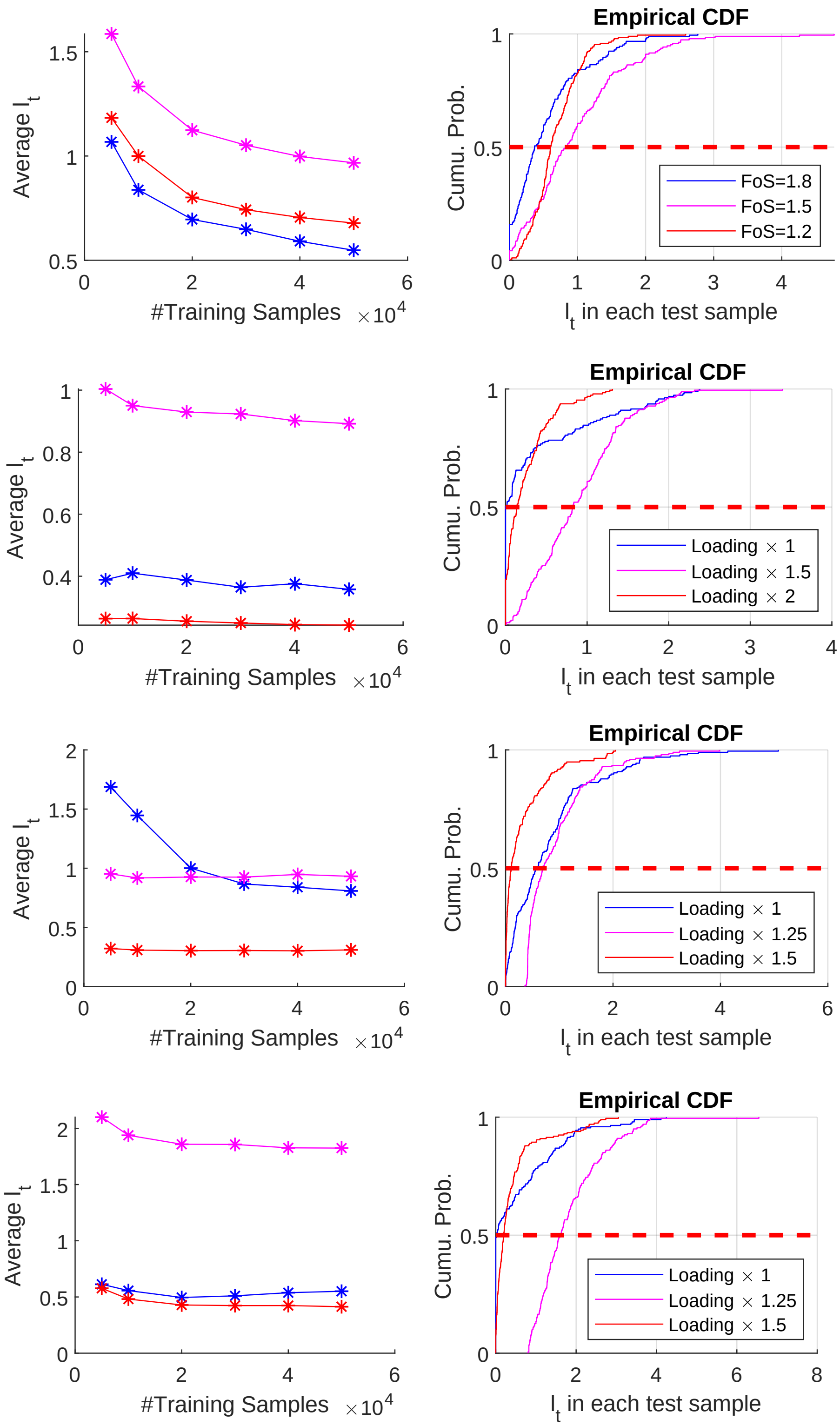

Figure 4-7: Results on l_t: 118, 1354, 2383, 3012-bus systems in order

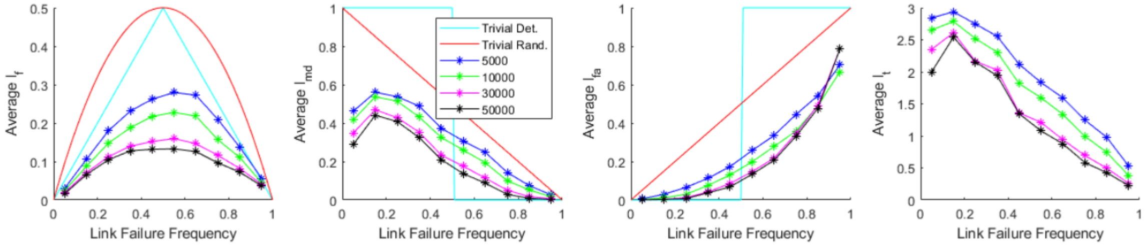

Figure 4-8: Results on each link for 118-bus DC system with FoS=1.5

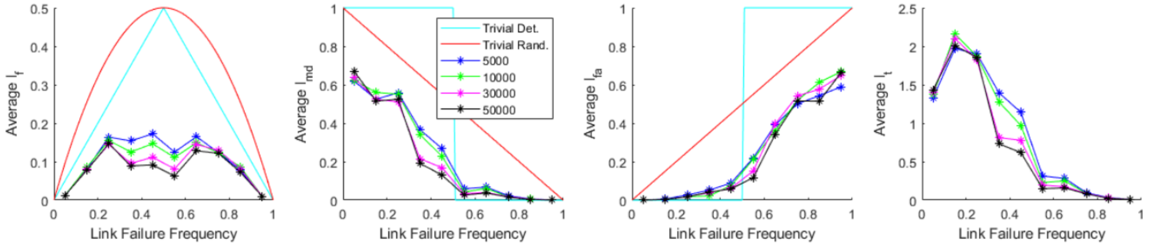

Figure 4-9: Results on each link for 1354-bus DC system with 2× default loading

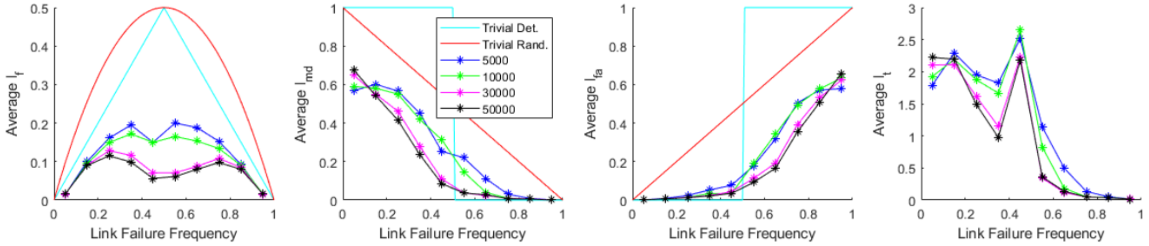

Figure 4-10: Results on each link for 2383-bus DC system with 1.5× default loading

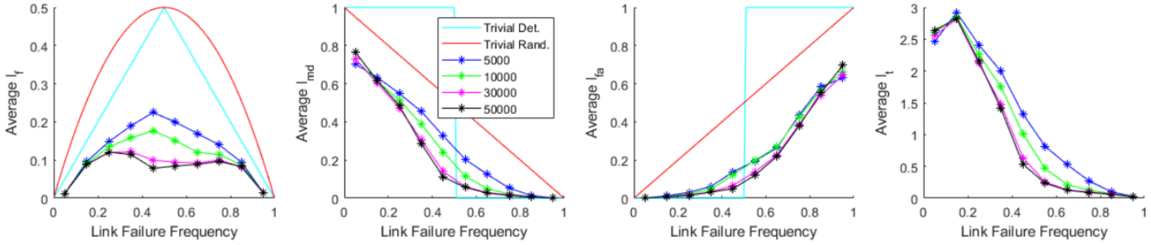

Figure 4-11: Results on each link for 3012-bus DC system with 1.5× default loading

be normal if its failure frequency is smaller than 50%. Randomized trivial prediction is to predict a link to be failed with probability equal to its failure frequency among the training samples under the corresponding setting. In each subfigure, we use the light blue curve to represent the deterministic one, and the red curve to represent the randomized one.

We explain the results on the four metrics in order.

- For the final state error rate $l_{f,i}$, we can observe that among all the failure frequency intervals, the prediction error based on the trained influence model is lower than that in the trivial methods. Meanwhile, with increasing number of training samples, $l_{f,i}$ in each interval decreases, especially for links with failure frequency around 50%. This shows that our prediction mechanism can effectively reduce the prediction error mostly for links that are hard to predict its final state by trivial methods.
- For the miss detection error rate $l_{md,i}$ and the false alarm error rate $l_{fa,i}$, they are in fact metrics with mirror symmetry to some extent. For $l_{md,i}$, the deterministic trivial method will have zero error rate for links with failure frequency higher than 50%, as it always predicts these links to be failed. In the opposite, the prediction error rate is 100% for the links with failure frequency lower than 50%. Comparing the trivial methods with our prediction mechanism, we can observe that the prediction based in influence model induces lower miss detection rate than the randomized naive method. Meanwhile, links with higher failure frequency leads to generally lower miss detection rate. This is because such links have experienced failures more frequently in the training set, which instructs the model to be prone to predict the failure of these links. In addition, the links with lower failure frequency itself fail less frequently, hence as we have mentioned, whenever we fail to identify one failure of it in the test set, the miss detection rate will be large. For the false alarm error rate $l_{fa,i}$, we will have similar analysis but opposite results, where links fail with high frequency generally lead to large false alarm rate. Therefore we should combine $l_{md,i}$ and

$l_{fa,i}$ together to evaluate the performance and explain the results.

- For the time error $l_{t,i}$, we also use the prediction error of time steps to represent. We can find that the prediction error for links with higher failure frequency is generally lower. The reason is similar to that for the miss detection: links fail with high frequency feeds more information about its failure to the model. Besides, the prediction error for links with lower failure frequency is large, as they tend to be predicted to be normal, and whenever it is predicted normal, the time prediction error is large. For example if the cascade lasts for 9 generations, our prediction on its time step is 10 (since it does not fail in the previous 9 generations) while the ground truth might be that this link fails at step 2, thus inducing an error of 8 time steps.

Besides, note that the performance in 118-bus system is sometimes inferior to larger systems. The reason is that in the 118-bus system, we set the link capacity values proportional to the link flow calculated by the loading and power generation, so the robustness is not ensured as that in large systems where capacity values are mostly provided officially. Therefore in 118-bus system, the cascading failures may even be more serious and thus harder to predict.

Summarizing the performance patterns in all the systems, we can draw that the trained influence model is really conducive to the failure cascade prediction compared with trivial methods, and it benefits most to the links whose failure is hard to predict in trivial methods.

4.5 Performance Evaluation on AC systems

The evaluation in AC systems is similar to that in DC systems. We consider both sample-based and link-based metrics, and consider different FoS and loading conditions. Due to the similar pattern as DC systems, we only present the result over three systems: 118-bus, 1354-bus, and 2383-bus systems. In each system we only consider two FoS/loading conditions: FoS$= 1.2, 1.5$ for 118-bus system; 1.5×, 2× default loading for 1354-bus systems; 1×, 1.25× default loading for 2383-bus systems.

4.5.1 Sample-based metrics

Fig. 4-12 to 4-14 show the result of the three sample-based metrics in 118-bus, 1354-bus, and 2383-bus system under AC flow, respectively the failure size error rate l_{size}, the final state error rate l_f, and the time prediction error l_t. In 118-bus system, we can observe that as we increase the training samples to 50,000, the failure size error rate can be reduced below 8%, the final state prediction error rate can be down to 12%, and the time prediction error is lower than 1 time step. Meanwhile, the CDF under 50,000 training samples informs us that most of the test samples can be predicted within reasonable range. In 1354-bus system, note that we only consider at most 5,000 cascade samples for training. This is because the cascade pattern under the AC flow model in this system is not complex, hence with 5,000 samples the prediction accuracy decreases to some stable level. In 2383-bus system, due to the heavy time burden to generate a cascade sample based on calculating the AC flow, we only present the results training at most 30,000 samples. In both of these two large systems, we can still observe a decreasing trend generally on all the metrics with more training samples.

Besides, by comparing the DC and AC system under the same capacity and loading conditions, we can find that the prediction performance in AC systems is a bit inferior to that in DC systems, which matches to the fact that the AC flow model is more complex.

4.5.2 Link-based metrics

Fig. 4-15 and 4-17 present the results of link-based metrics in 118-bus and 2383-bus system under AC flow. Similar in the trend compared with DC cases, we can find that prediction based on the trained influence model is much more accurate than the trivial methods, and more training samples will reduce the error rate among all these four metrics. The performance is also inferior compared with that under DC flow

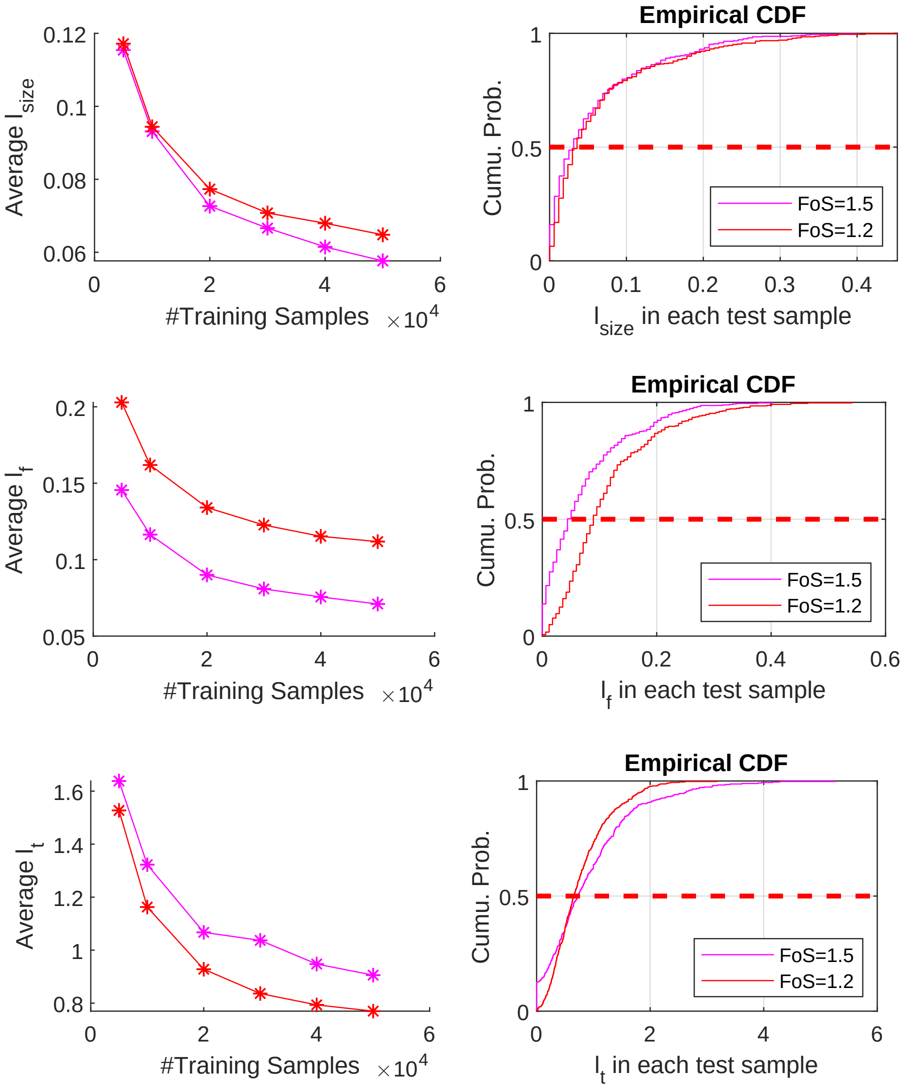

Figure 4-12: Results on l_{size}, l_f, l_t in order for 118-bus AC system

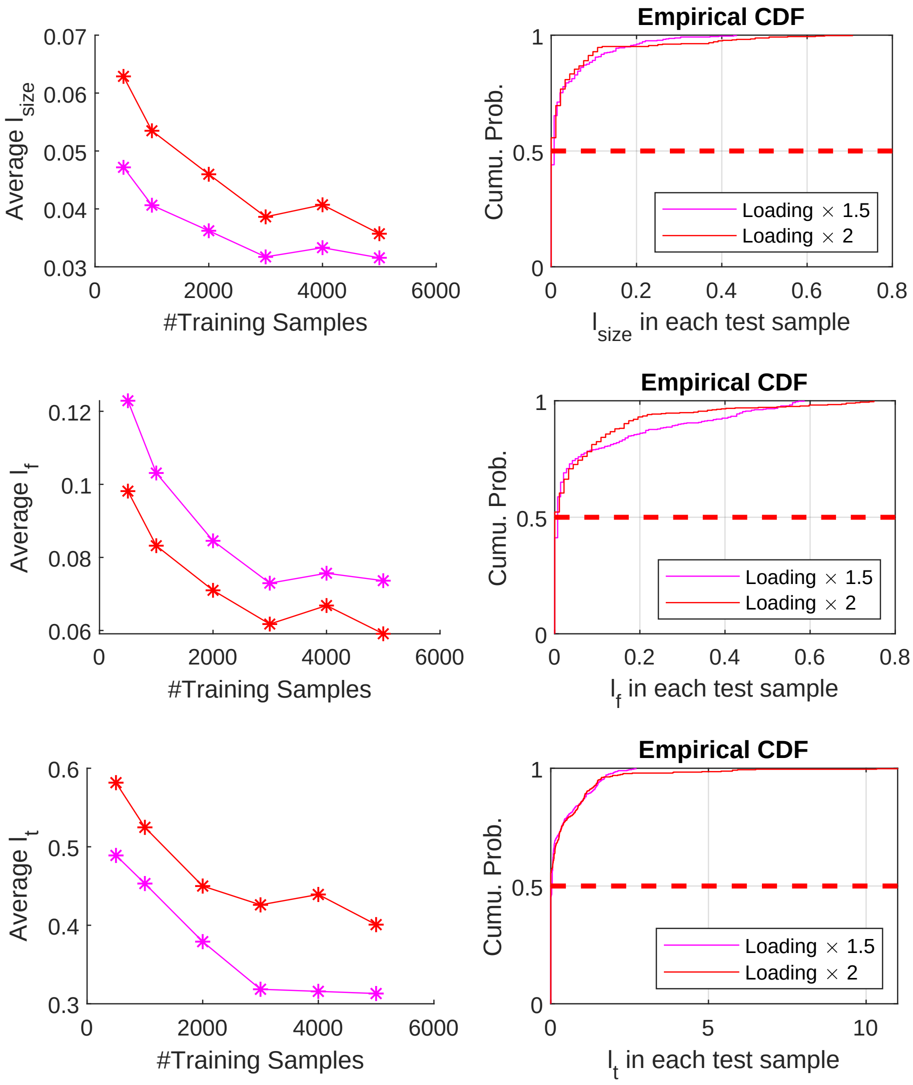

Figure 4-13: Results on l_{size}, l_f, l_t in order for 2383-bus AC system

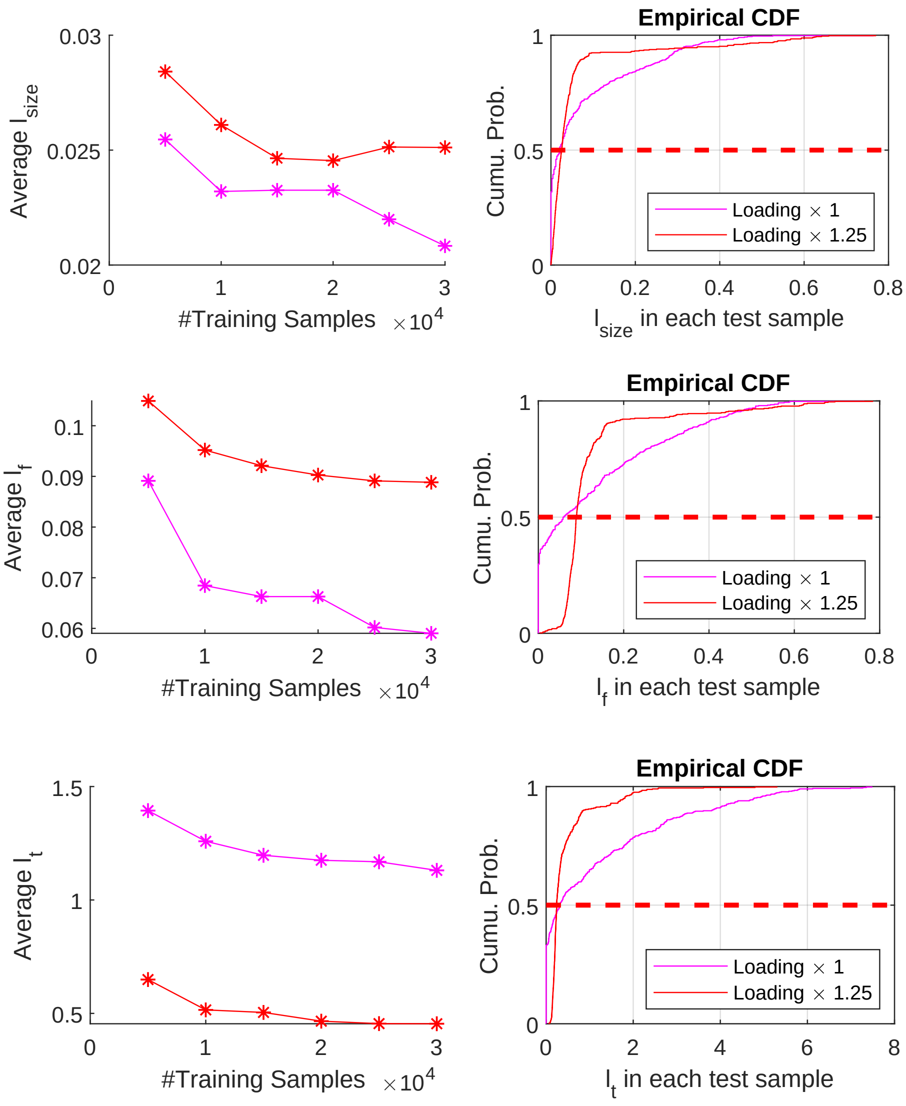

Figure 4-14: Results on l_{size}, l_f, l_t in order for 2383-bus AC system

under the same condition.

Three additional things should be noted. (i) We lack the miss detection rate for links with failure frequency less than 10% in 118-bus system under AC flow. This is because these links do not experience any cascading failure, i.e, their failure frequency is 0. (ii) No links have failure frequency between 20% and 60% in 1354-bus system under AC flow. (iii) Under both DC and AC cases, while we increase the number of training samples, the miss detection rate for links fail with low frequency may even be larger than that under fewer training samples, and similar in the false alarm rate for links fail with high frequency. For the miss detection, it may be because for the links that rarely fail, more training samples may furthermore 'dilutes' the cases of the cascading failure on such links, hence leading the prediction of the final state of such links to be normal and thus arousing even larger miss detection rate. The interpretation on false alarm rate is similar.

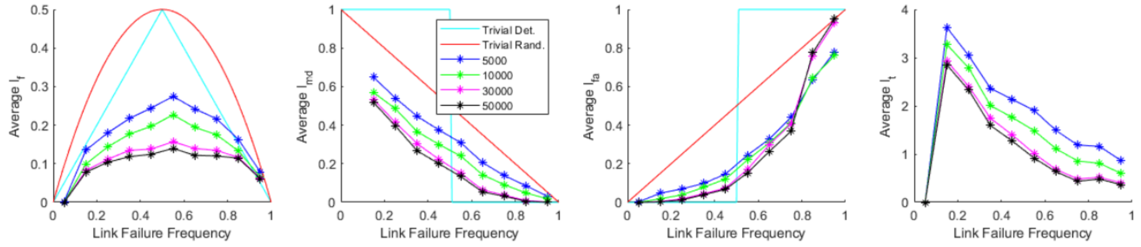

Figure 4-15: Results on each link for 118-bus AC system with FoS=1.2

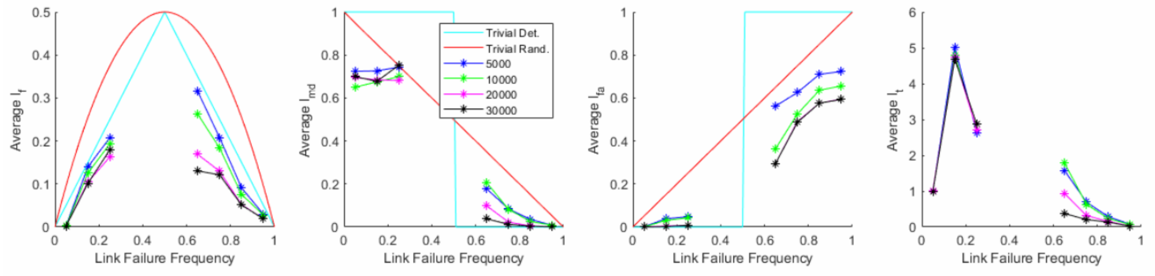

Figure 4-16: Results on each link for 1354-bus AC system with 2× default loading

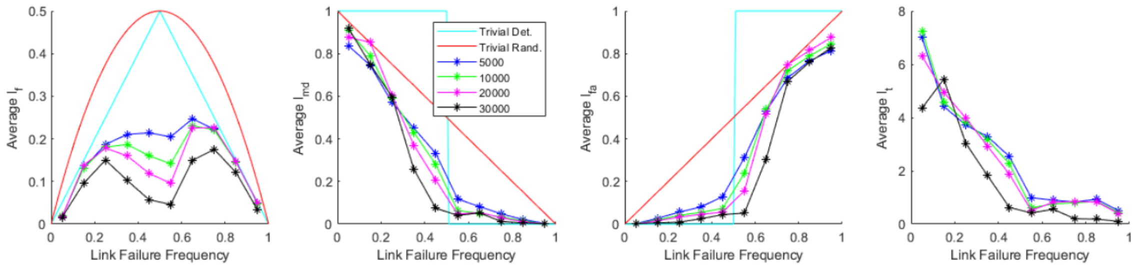

Figure 4-17: Results on each link for 2383-bus AC system with 1× default loading

4.6 Prediction Time Comparison

Further, we show the superiority of the influence model based prediction to power flow calculation by MATPOWER Toolbox in time cost reduction under both DC and AC flow. Specifically, we test both methods in MATLAB 2019a on Intel(R) Core(TM) i9-7920X CPU@2.90GHz Processor with 128GB installed memory. In each setting, we run $1,000$ test sample via each method and compute its total time cost.

We summarize the results of DC systems in Table 4.3 and AC systems in Table 4.4. We use '$a \mid b \mid \mathbf{c}$' structure to present our results, where a denotes total number of seconds by flow calculation, b denotes total number of seconds by our method, and $\mathbf{c} = a/b$, reflecting how many times faster the influence model-based method is compared to the traditional power flow method. Results show that our method works better in larger systems and under higher loading conditions that tend to cause large failures, which demonstrates its effectiveness and scalability. For example, the time cost by our method is 1/136 of that by flow calculation under medium loading in the 3012-bus system in DC flow setting. The main reason is that more islands appears under these conditions, which requires to solve DC flow equations for more times, while the prediction by influence model discards all such calculations.

By comparing the results in DC and AC systems, we can find that the time cost gap between our method and the simulation-based method is even larger. The main reason is that the dynamics of AC systems is more complex: during flow calculation, the flow calculation sometimes needs to do load shedding multiple times until it finds a convergent solution, and it is done by Newton-Raphson method instead of simply solving linear equations. However, our method does not incorporate these more complex processes, hence the time cost keeps nearly the same as that in DC systems, which is only determined by the number of cascade generations we predict.

Table 4.3: Prediction Time Cost on 1,000 Samples in DC Systems

	Low Load	Medium Load	High Load
1354-bus	808 | 21.3 | **38**	1930 | 19.8 | **97**	1740 | 19.6 | **89**
2383-bus	2597 | 43.3 | **60**	3490 | 37.8 | **92**	3603 | 34.7 | **104**
3012-bus	3891 | 59.4 | **66**	8020 | 58.9 | **136**	5864 | 46.9 | **125**

Table 4.4: Prediction Time Cost on 1,000 Samples in AC Systems

	Low Load	High Load
1354-bus	5280 | 24.9 | **212**	4950 | 23.5 | **211**
2383-bus	14498 | 34.4 | **421**	29197 | 33.5 | **872**

Chapter 5

Cascade Property Analysis

In this section, we probe into the insights that the influence model trained by the hybrid learning framework can offer, which we cannot directly obtain from observation. We firstly observe that the main influence in power systems is very sparse, and further quantify the relationship between influence and physical distance among two links. Then we identify critical initial contingencies simply based on the trained parameters $\{\mathbf{A}^{11}, \mathbf{A}^{01}, \mathbf{D}, \epsilon\}$. Such analysis uncovers broader usage of the influence model.

5.1 Influence Sparsity

A very interesting observation of the influence model is that the learned matrix $\mathbf{D}$ by (3.5) appears to be *sparse*, where most of the elements are very close to 0. This means that in power systems, each link is mainly influenced by very small number of other links. To study on this phenomenon, we test on 118-bus and 2383-bus cases under DC flow, and show the spatial distribution of $\mathbf{D}$ values that are larger than 0.01 in Fig. 5-1. We define an influence to be *visible* from link i to j if $d_{ji} > 0.01$. Note that there are 310 and 9904 visible influences in each system respectively. Under such setting, as there are 171 and 2088 effective links respectively in 118-bus and 2383-bus systems, hence in each row of $\mathbf{D}$, there are averagely $310/171 = 1.8$ and $9904/2088 = 4.7$ visible influences, accounting for $1.8/179 = 1.0\%$ and $4.7/2886 = 0.2\%$ among all links in each system (note that ineffective links may also fail initially to affect others).

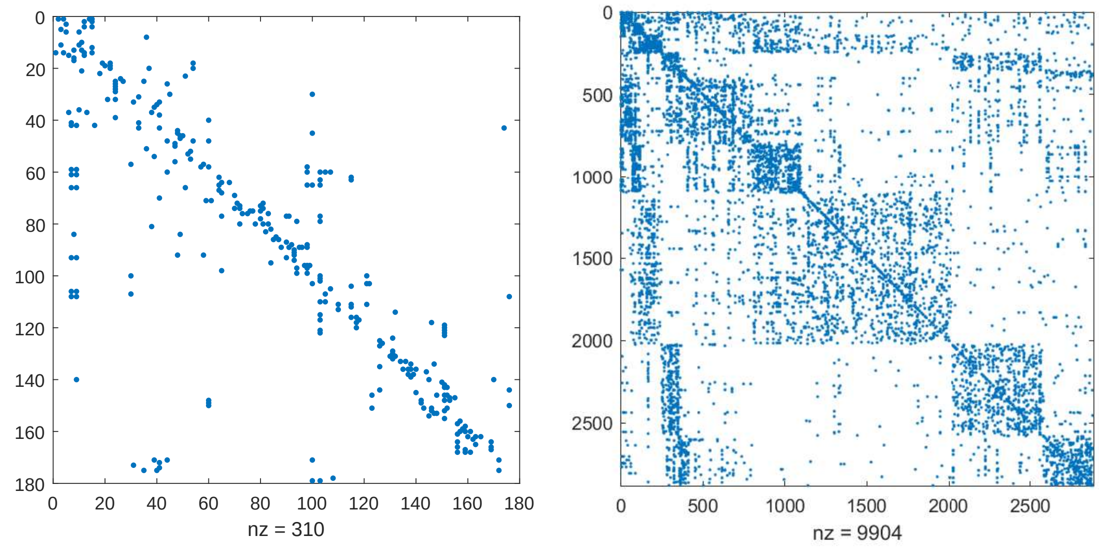

(a) 118-bus

(b) 2383-bus

Figure 5-1: Spatial distribution of **D** values larger than 0.01 in 118-bus and 2383-bus system in default setting under DC flow.

Based on the sum of each row in **D** is 1, the result indicates that only very few links dominate the influence on a specific link. In all, network influence can be sparse enough to represent most of correlation within the power systems.

Additionally, we can observe that **D** is generally but not completely symmetric in terms of its diagonal, which implies that the influence between two links are not always bidirectional. Meanwhile, many visible influences are gathering around diagonals, and based on indexing rule [32], many adjacent links have very close link indexes, hence the result shows that the local influence is still a major role in power networks. To this observation, we will show in next part with more details by quantifying the relationship between the influence values and the physical distance between transmission links, a step further than focusing solely on links adjacent or not.

5.2 Relationship between Influence and Distance

Indicated by Kirchhoff's law, adjacent links should be correlated more tightly, hence share a stronger influence. However, as capacity values vary among different links, the cascade process may not follow in this way. In this part we explore the relationship between the influence value and physical distance between any pair of links. The influence is characterized by $\mathbf{D}$, $\mathbf{A}^{11}$ and $\mathbf{A}^{01}$. Based on (2.1), we can find that

$$\tau_{ij} \overset{\triangle}{=} d_{ij}(\mathbf{A}^{11}_{ji} - \mathbf{A}^{01}_{ji})$$

reflects the *total influence value* from link j to i, as when $s_j[t]$ turns from 1 to 0, the value of $\tilde{s}_i[t+1]$ will be decreased by such total influence value. Here we term the total influence from link j to link i is *visible* if $\tau_{ij} > 0.01$. The physical distance is defined as the minimum topologically hops between two links. For example, if link i and j are adjacent, then the distance between them is 1; if they are not but connected by another common link k, then the distance between link i and j is 2.

We present the results over 118-bus and 1354-bus systems under DC systems and their default settings in Table 5.1, Fig. 5-2 and 5-3. Table 5.1 lists our measurement on 4 aspects on both systems: the total number of link pairs with a specific distance (#LinkPairs), the rate of visible link pairs compared with all those under such distance (Vis. rate), the average of τ among all link pairs ($\mathbf{E}[\tau]$), and that among all visible ones ($\mathbf{E}[\text{Vis. } \tau]$). We use '$a \mid b$' structure to present the result in 118-bus and 1354-bus systems respectively. Fig. 5-2 and 5-3 illustrate the distribution of τ values larger than 0.01, where the abscissa axis denotes different τ values. We discard the part where $\tau < 0.01$ as it takes very large proportion, implied in the discussion about influence sparsity in the last section. Including this part will make the distribution concentrate near 0.

Such truncation, however, does not matter, as Fig. 5-2 and 5-3, together with Table 5.1, can present all the related information. For example, in 118-bus case, suppose we consider links that have distance 1, then there are $1018 \times 11.8\% \approx 120$ visible link pairs. Then by Fig. 5-2, we can calculate that the number of link pairs whose total influence τ is within $(0.5, 0.55)$ should be $120 \times 1.67\% = 2$. From the records, especially the column ($\mathbf{E}[\text{Vis. } \tau]$) in Table 5.1, we can figure out that in both systems, the major influence still exists in adjacent link pairs, and as distance becomes larger, the influence values decline generally but does not approach 0. This shows that under both capacity settings, local influence is stronger while far-away influence can never be neglected.

Table 5.1: Influence-Distance Analysis Results for 118|1354-Bus System in Default Setting.

	#LinkPairs	**Vis. Rate**	**E[τ]**	**E[Vis. τ]**
System Size	**118 | 1354**	**118 | 1354**	**118 | 1354**	**118 | 1354**
Dist.= 1	1018 | 10242	11.8% | 2.4%	.030 | 0.003	0.25 | 0.33
Dist.= 2	2166 | 22892	4.2% | 1.4%	.007 | 0.003	0.16 | 0.26
Dist.= 3	3180 | 42308	1.2% | 0.7%	.002 | 0.001	0.15 | 0.21
Dist.= 4	3810 | 71360	0.5% | 0.4%	.001 | 0.001	0.13 | 0.16

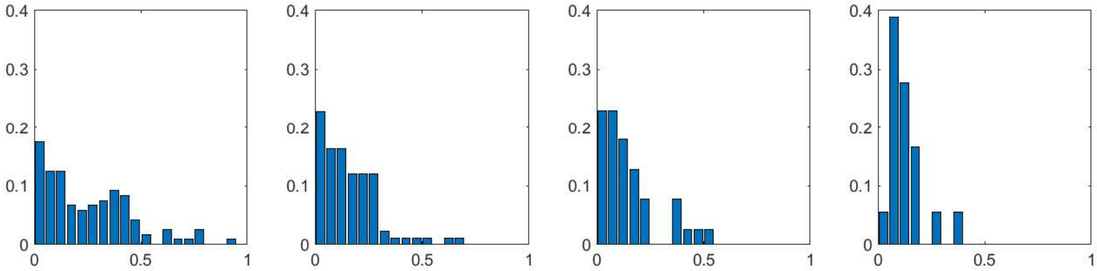

Figure 5-2: Visible Influence Value Distribution in 118-Bus System.

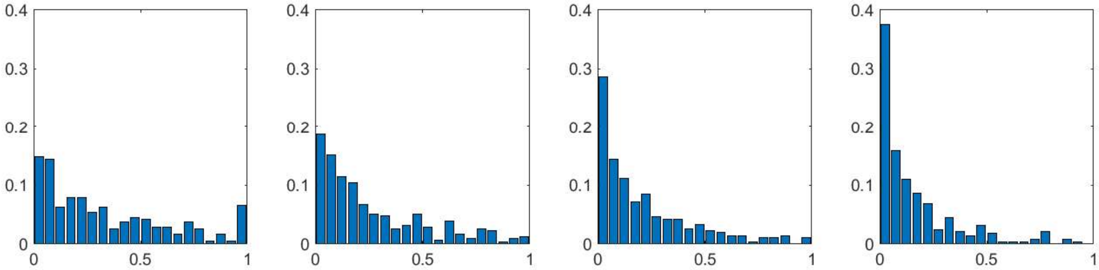

Figure 5-3: Visible Influence Value Distribution in 1354-Bus System.

5.3 Critical Initial Contingency Identification

In this section, we explore new applications based on our trained model. We consider whether it can be used to identify the critical $M-k$ initial contingencies that can arouse failure cascade with large size.

Intuitively based on (2.1), a link whose failure that has enormous negative effects on the whole system should greatly reduce the intermediate state values $\tilde{s}[t]$ of other links during the cascade, as this will drag the value $\tilde{s}_i[t]$ down below the threshold values ϵ_i for each link i with higher chances generally. Therefore, a natural idea to identify the links that may cause large failure size is to find the link j^* such that

$$j^* = \arg\max_j \sum_{i=1}^{M} \tau_{ij} = \arg\max_j \sum_{i=1}^{M} d_{ij}(\mathbf{A}_{ji}^{11} - \mathbf{A}_{ji}^{01}). \tag{5.1}$$

where $\tau_{ij} \triangleq d_{ij}(\mathbf{A}_{ji}^{11} - \mathbf{A}_{ji}^{01})$ reflects the synthesized influence from link j to i based on (2.1), as it combines both pairwise influences and the weights. When $s_j[t]$ turns from 1 to 0, the value of $\tilde{s}_i[t+1]$ is decreased by τ_{ij}. We define the sum $\sum_{i=1}^{M} \tau_{ij}$ as the *total influence* of link j on the whole system. Intuitively, the link j^* with highest total influence value is the link we predict whose failure is most prone to cause large failures. We can find the top-L links $\{j_l\}_{l=1}^{L}$ that maximize $\sum_{i=1}^{M} \tau_{ij}$. Any $M-k$ initial contingency among these L links, in our expectation, should arouse large failure size.

One question arises naturally that what value of L we should choose in each system. The idea we implement is that we sort the total influence value $\sum_{i=1}^{M} \tau_{ij}$ for each link j in increasing order, as shown in Fig. 5-4 for the three systems we tested: 118-bus, 1354-bus, and 2383-bus systems. We can observe that there are approximately 10 to 15 links that have apparently larger total influence value than other links, while the total influence value of most of the links is close to 0. Therefore we take top 10 to 15 links according to (5.1), and similarly the bottom 10 to 15 links.

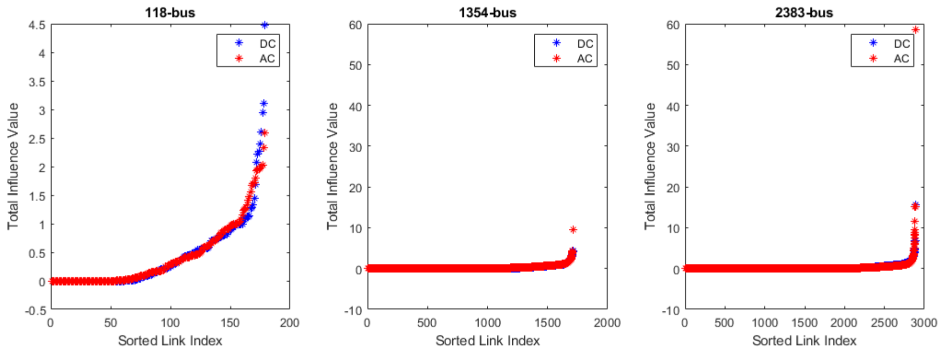

Figure 5-4: Link indexes sorted based on total influence values for the three tested systems

To verify whether this scheme works, we first test on the 118-bus system under both DC and AC flow. For DC flow, we consider FoS being 1.5 and 1.8. In each setting, we construct $50,000$ cascade sequences and obtain the empirical distribution of ultimate failure size, denoted as p_0. Then we find top 10 links that maximize/minimize $\sum_{i=1}^{M} \tau_{ij}$ in terms of j, denoted as $J_{max} \triangleq \{j_l^{max}\}_{l=1}^{10}$ and $J_{min} \triangleq \{j_l^{min}\}_{l=1}^{10}$ respectively. For J_{max}, we enumerate all $M-k$ contingencies where initially failed links are all in J_{max}, and find the empirical failure size distribution p_{max}. For example, if $k=3$, then it involves $\binom{10}{3}$ initial outage combinations. Similarly we can obtain p_{min} from J_{min}. By comparing p_{max}, p_{min} with p_0, we can directly figure out whether our choices of J_{max} and J_{min} based on the trained influence model can really identify the most critical and non-critical $M-k$ initial contingencies.

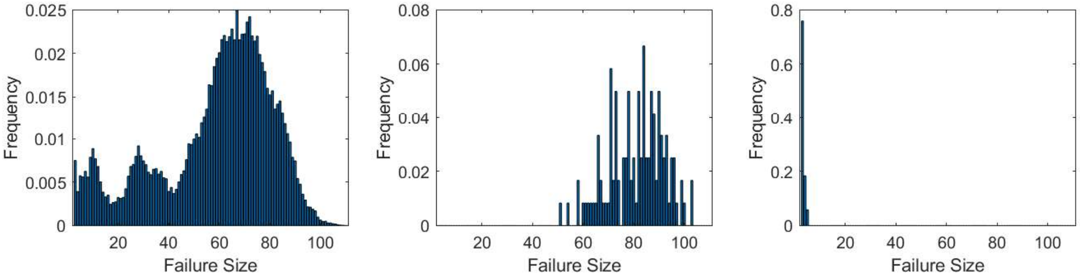

Figure 5-5: Failure Size Distribution for 118-Bus FoS=1.5 (DC).

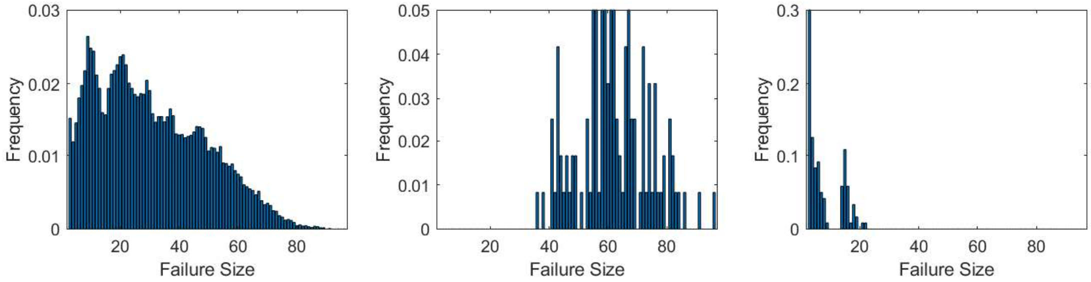

Figure 5-6: Failure Size Distribution for 118-Bus FoS=1.8 (DC).

Fig. 5-5 and 5-6 present the results for 118-bus case under DC flow. The leftmost subfigure shows the empirical failure size distribution p_0, while the middle and rightmost reflect p_{max} and p_{min} respectively. We can observe that in both cases, p_{max} tilts to the large failure size, with mean size 81 and 62, while p_{min} concentrates on very small failure size, with mean size 11 and 8 in these two settings respectively. The violent difference between p_{max} and p_{min} demonstrates the validity of our method to clearly distinguish the initial contingencies that are critical and non-critical. Fig. 5-7 shows the results over AC flow case where FoS= 1.8. We can find that it can also identify the initial contingencies that will lead to large and small cascade failure size. However its identification is not so accurate as that in DC flow, which matches to the fact that AC dynamics is more complex to capture and remains to be further enhanced in future.

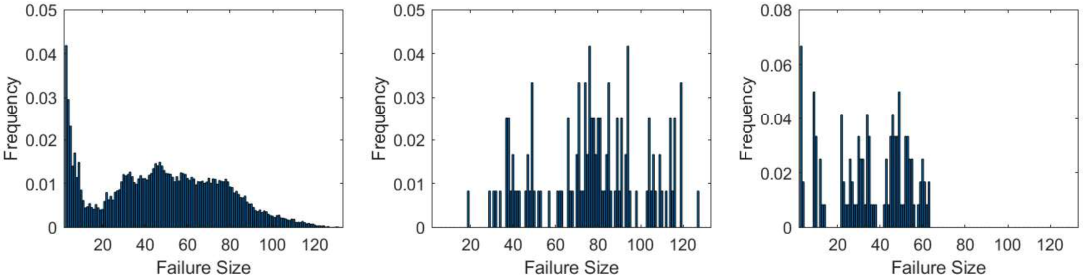

Figure 5-7: Failure Size Distribution for 118-Bus FoS=1.5 (AC).

Furthermore, we show the spatial distribution of J_{min} and J_{max} for both FoS conditions in 118-bus system in Fig. 5-8(a) and 5-8(b). The yellow links are 10 most critical links, while the green ones are the 10 most non-critical. For the two loading conditions, some links keep to be critical, while there also exists some difference in the links. This can tell us the links consistently critical under load fluctuation. Meanwhile, the critical links are spatially remote from each other, indicating that local management is not enough to identify them.

Further we extend the critical initial contingency identification to 1354-bus and 2383-bus systems under both DC and AC flow model. In these cases, we set the capacity value of each link as 1.5 times the flow on it under the default power generation and loading level, as we have done in the 118-bus system. The results are shown in Fig. 5-9 to Fig. 5-12, where in each figure, the left subfigure represents the distribution of failure size among the training cascade sequences, while the middle one represents the failure size distribution induced by M-2 initial contingencies over the top-15 links we select based on (5.1), and the right on represents that over the bottom-15 links. We can observe that this method can also distinguish out the initial

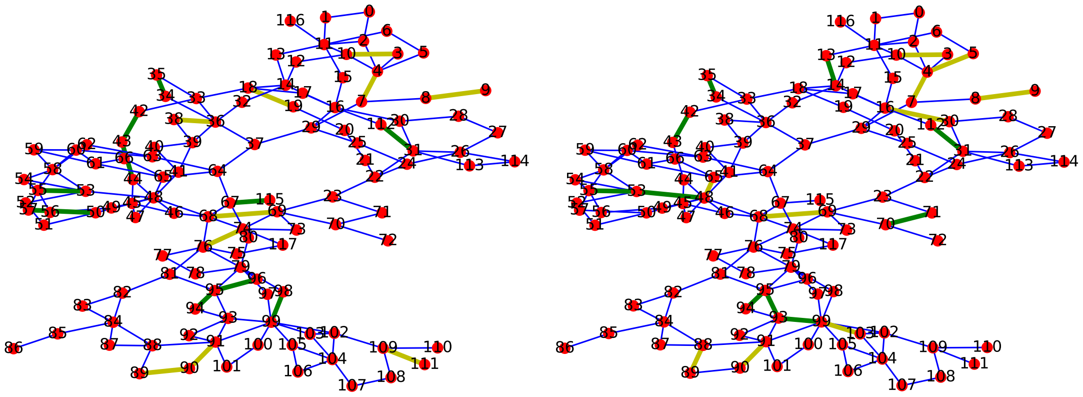
(a) (b)

Figure 5-8: Spatial Distribution of Critical/Non-Critical Links in 118-Bus System under DC flow: (a) FoS=1.5, (b) FoS=1.8

contingencies that will arouse the most/least serious failure cascade clearly, and it is more accurate in DC system than that in AC system as well.

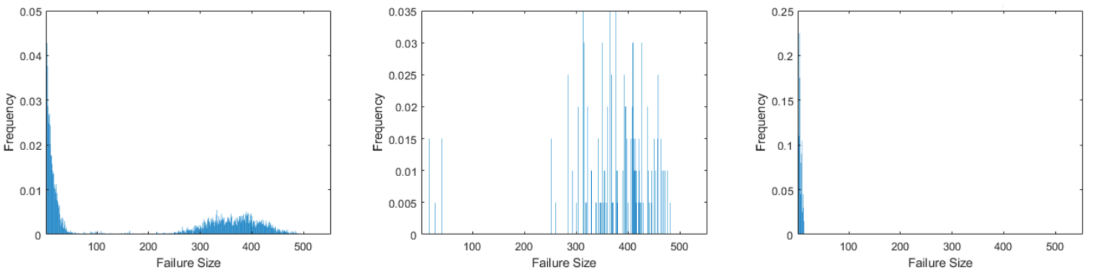

Figure 5-9: Failure Size Distribution for 1354-Bus FoS=1.5 (DC).

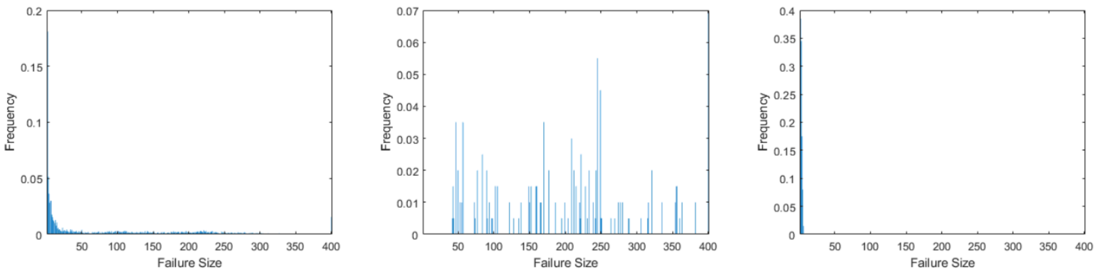

Figure 5-10: Failure Size Distribution for 1354-Bus FoS=1.5 (AC).

We further test the scheme on 1354-bus and 2383-bus systems under the provided link capacity value. In this case, we compare p_0 and p_{max} to show whether this framework can still identify the critical initial contingencies that lead to severe failure

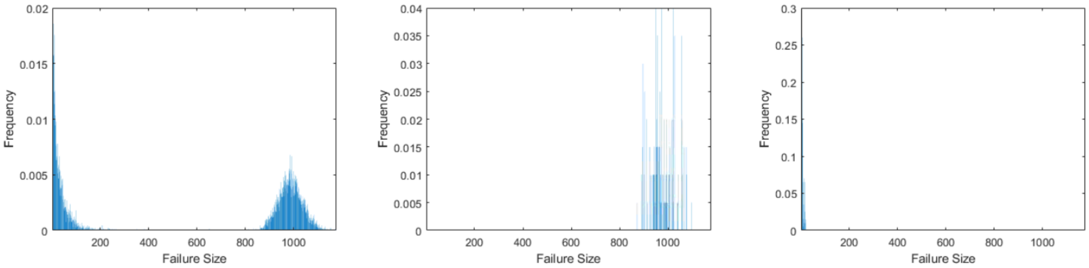

Figure 5-11: Failure Size Distribution for 2383-Bus FoS=1.5 (DC).

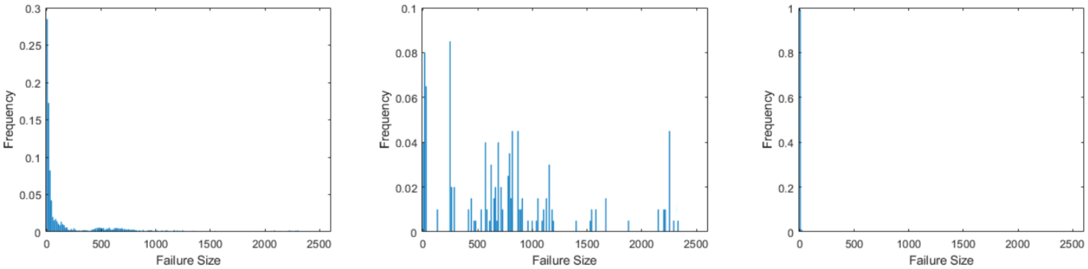

Figure 5-12: Failure Size Distribution for 2383-Bus FoS=1.5 (AC).

cascade. For p_{max} we also consider the top-10 links with largest total influence value.

Fig. 5-13 presents the results for both systems under DC flow model. The blue bars represent p_0, while the orange bars represent p_{max}. We can observe that in both cases, p_{max} tilts to the large failure size and contains larger failure size with higher ratio, which indicates that the selection of the top-10 influential links by (5.1) tends to induce larger failure size compared with randomly tripping 2 links initially.

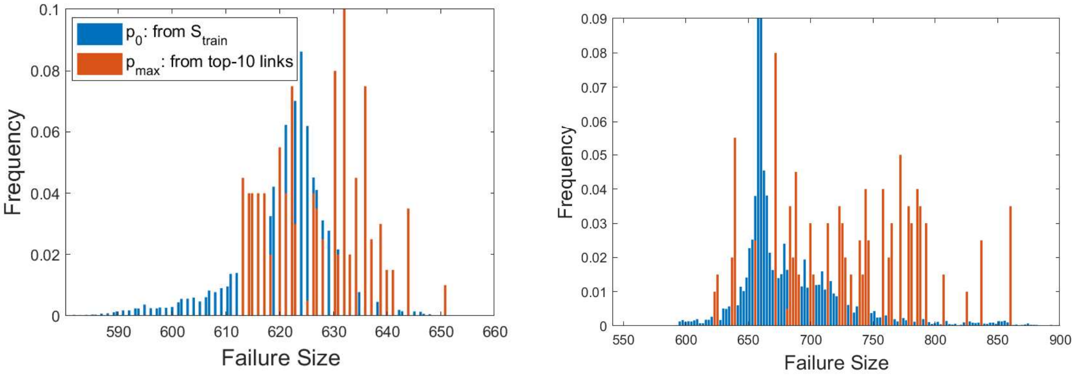

Figure 5-13: $M-2$ cascade failure distribution of S_{train} and top-10 influential links in DC systems (Left: 1354-bus, 2× default loading; Right: 2383-bus 1.25× default loading)

Fig. 5-14 and Fig. 5-15 present the results over AC flow case with different loading conditions for 1354-bus and 2383-bus systems respectively. In 1354-bus system, under both loading conditions, the top-10 links we select can identify higher portion of initial contingencies that lead to larger cascade size than that by random selection. However the identification under AC flow is not so accurate as that under DC flow, as higher portion of $M-2$ initial contingencies from the top-10 links will lead to failure size smaller than the average level of that in $\mathcal{S}_{train}$. This matches to the fact that AC dynamics is more complex to capture and remains to be further enhanced in future.

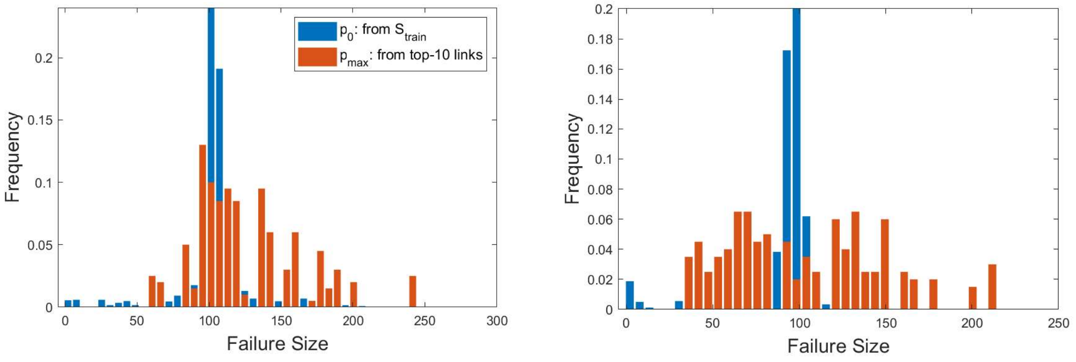

Figure 5-14: $M-2$ cascade failure distribution of S_{train} and top-10 influential links in 1354-bus AC system (Left: 1.5× default loading; Right: 2× default loading)

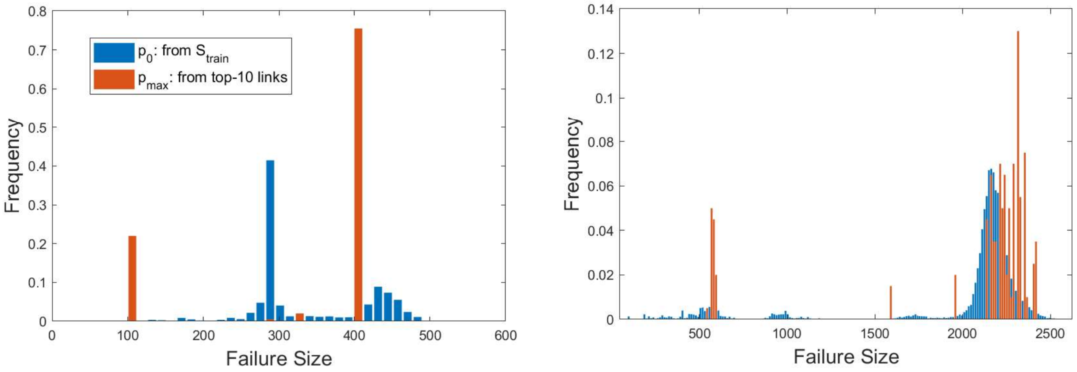

Figure 5-15: $M-2$ cascade failure distribution of S_{train} and top-10 influential links in 2383-bus AC system (Left: 1× default loading; Right: 1.25× default loading)

Table 5.2 presents the results in a more quantified manner. For each of the six settings discussed above, we calculate the ratio of $M-2$ initial contingencies in J_{max} whose failure size is no smaller than the median (1/2-quantile) value and 3/4-quantile value of that in $\mathcal{S}_{train}$. Such ratios are denoted as $\gamma_{1/2}$ and $\gamma_{3/4}$ respectively. The reference values are $\gamma_{1/2} = 50\%$ and $\gamma_{3/4} = 25\%$. If such ratios under the six settings are larger than the reference values, then it demonstrates that the mechanism based on (2.1) can effectively identify the critical initial contingencies. We can observe that $\gamma_{1/2} > 50\%$ for all the settings, and for $\gamma_{3/4}$, it largely surpasses 25% in all the cases except '2383AC (1×)'. In fact, for this setting, shown in Fig. 5-15, we can show that its $\gamma_{2/3} = 75.5\%$. The results verify that our mechanism works in broad settings as well.

Table 5.2: $\gamma_{1/2}$ and $\gamma_{3/4}$ of all the six settings under our mechanism

Ratio	p_0	p_{max}		
	All Systems	1354DC (2x)	1354AC (1.5x)	1354AC (2x)
$\gamma_{1/2}$	50%	68%	71.5%	55%
$\gamma_{3/4}$	25%	57%	66%	55%
Ratio	p_0	p_{max}		
	All Systems	2383DC (1.25x)	2383AC (1x)	2383AC (1.25x)
$\gamma_{1/2}$	50%	87.5%	78%	73.5%
$\gamma_{3/4}$	25%	67.5%	0%	60.5%

In addition, the identification of critical initial contingencies is purely based on the influence model trained by our framework, with no addition information needed, such as bus loading and link flow. Moreover, its time complexity is $O(M)$, thus efficient enough to operate on large systems.

Chapter 6

Conclusion and Future Work

In this thesis, we build an influence model framework to study and predict failure cascades in large scale power systems. We propose a hybrid learning scheme to train the influence model based on simulated failure cascade samples. Experimental results on large scale power systems demonstrate acceptable prediction performance over metrics with different levels of evaluation granularity, and we further show that our method bears a significant time cost reduction compared with power flow simulation based approach. In addition, we show that the influence model trained by the hybrid framework can reflect cascade properties such as influence sparsity, the relationship between influence and physical distance, and the critical and non-critical initial contingencies.

However, some unsolved issues still exist in our methodology. For example, when a link rarely fails, it is hard to identify its failure based on the current learning framework without additional operations, and thus leading to high miss detection rate. Improving the training structure in order to better account for rare events is an important direction of future work. Moreover, the application of this framework into other network systems, including communication systems and even interdependent network systems, is worth investigation, as this learning framework over influence model does not rely on any specific network model.

Bibliography

[1] "NorthEast US Failure Cascade." https://www.bostonglobe.com/magazine/2012/02/03/anatomy-blackout-august/mAsrr41nLAjGFIU3IF440O/story.html.

[2] "Manhattan, New York Failure Cascade." https://www.theatlantic.com/technology/archive/2019/07/manhattan-blackout-reveals-infrastructure-risk/594025/.

[3] "London Failure Cascade." https://www.bloomberg.com/news/articles/2019-08-09/london-blackout-occurred-amid-drop-in-wind-and-natural-gas-power.

[4] Z. Wang, M. Rahnamay-Naeini, J. M. Abreu, R. A. Shuvro, P. Das, A. A. Mammoli, N. Ghani, and M. M. Hayat, "Impacts of operatorsąŕ behavior on reliability of power grids during cascading failures," *IEEE Transactions on Power Systems*, vol. 33, no. 6, pp. 6013–6024, 2018.

[5] H. Cetinay, S. Soltan, F. A. Kuipers, G. Zussman, and P. Van Mieghem, "Comparing the effects of failures in power grids under the ac and dc power flow models," *IEEE Transactions on Network Science and Engineering*, vol. 5, no. 4, pp. 301–312, 2017.

[6] A. Bernstein, D. Bienstock, D. Hay, M. Uzunoglu, and G. Zussman, "Power grid vulnerability to geographically correlated failuresąłanalysis and control implications," in *IEEE INFOCOM 2014-IEEE Conference on Computer Communications*, pp. 2634–2642, IEEE, 2014.

[7] A. Bernstein, D. Bienstock, D. Hay, M. Uzunoglu, and G. Zussman, "Sensitivity analysis of the power grid vulnerability to large-scale cascading failures," *ACM SIGMETRICS Performance Evaluation Review*, vol. 40, no. 3, pp. 33–37, 2012.

[8] S. Soltan, D. Mazauric, and G. Zussman, "Analysis of failures in power grids," *IEEE Transactions on Control of Network Systems*, vol. 4, no. 2, pp. 288–300, 2015.

[9] S. Soltan, A. Loh, and G. Zussman, "Analyzing and quantifying the effect of k-line failures in power grids," *IEEE Transactions on Control of Network Systems*, vol. 5, no. 3, pp. 1424–1433, 2017.

[10] Z. Kong and E. M. Yeh, "Correlated and cascading node failures in random geometric networks: A percolation view," in *2012 Fourth International Conference on Ubiquitous and Future Networks (ICUFN)*, pp. 520–525, IEEE, 2012.

[11] H. Xiao and E. M. Yeh, "Cascading link failure in the power grid: A percolation-based analysis," in *2011 IEEE International Conference on Communications Workshops (ICC)*, pp. 1–6, IEEE, 2011.

[12] Z. Wang, D. Zhou, and Y. Hu, "Group percolation in interdependent networks," *Physical Review E*, vol. 97, no. 3, p. 032306, 2018.

[13] C. Asavathiratham, S. Roy, B. Lesieutre, and G. Verghese, "The influence model," *IEEE Control Systems Magazine*, vol. 21, no. 6, pp. 52–64, 2001.

[14] M. Rahnamay-Naeini, Z. Wang, N. Ghani, A. Mammoli, and M. M. Hayat, "Stochastic analysis of cascading-failure dynamics in power grids," *IEEE Transactions on Power Systems*, vol. 29, no. 4, pp. 1767–1779, 2014.

[15] P. Das, R. A. Shuvro, Z. Wang, M. R. Naeini, N. Ghani, and M. M. Hayat, "Stochastic failure dynamics in communication network under the influence of power failure," in *2017 IEEE 13th International Conference on Wireless and Mobile Computing, Networking and Communications (WiMob)*, pp. 1–8, IEEE, 2017.

[16] R. A. Shuvro, Z. Wang, P. Das, M. R. Naeini, and M. M. Hayat, "Modeling impact of communication network failures on power grid reliability," in *2017 North American Power Symposium (NAPS)*, pp. 1–6, IEEE, 2017.

[17] P. D. Hines, I. Dobson, and P. Rezaei, "Cascading power outages propagate locally in an influence graph that is not the actual grid topology," *IEEE Transactions on Power Systems*, vol. 32, no. 2, pp. 958–967, 2016.

[18] K. Zhou, I. Dobson, Z. Wang, A. Roitershtein, and A. P. Ghosh, "A markovian influence graph formed from utility line outage data to mitigate cascading," *arXiv preprint arXiv:1902.00686*, 2019.

[19] M. Vaiman, K. Bell, Y. Chen, B. Chowdhury, I. Dobson, P. Hines, M. Papic, S. Miller, and P. Zhang, "Risk assessment of cascading outages: Methodologies and challenges," *IEEE Transactions on Power Systems*, vol. 27, no. 2, p. 631, 2012.

[20] H. Cetinay, S. Soltan, F. A. Kuipers, G. Zussman, and P. Van Mieghem, "Analyzing cascading failures in power grids under the ac and dc power flow models," *ACM SIGMETRICS Performance Evaluation Review*, vol. 45, no. 3, pp. 198–203, 2018.

[21] D. Bienstock and A. Verma, "The nk problem in power grids: New models, formulations, and numerical experiments," *SIAM Journal on Optimization*, vol. 20, no. 5, pp. 2352–2380, 2010.

[22] J. Zhang, E. Yeh, and E. Modiano, "Robustness of interdependent random geometric networks," *IEEE Transactions on Network Science and Engineering*, 2018.

[23] I. Dobson, "Estimating the propagation and extent of cascading line outages from utility data with a branching process," *IEEE Transactions on Power Systems*, vol. 27, no. 4, pp. 2146–2155, 2012.

[24] H. Ren and I. Dobson, "Using transmission line outage data to estimate cascading failure propagation in an electric power system," *IEEE Transactions on Circuits and Systems II: Express Briefs*, vol. 55, no. 9, pp. 927–931, 2008.

[25] M. J. Eppstein and P. D. Hines, "A ąřrandom chemistryąś algorithm for identifying collections of multiple contingencies that initiate cascading failure," *IEEE Transactions on Power Systems*, vol. 27, no. 3, pp. 1698–1705, 2012.

[26] P. Rezaei, P. D. Hines, and M. J. Eppstein, "Estimating cascading failure risk with random chemistry," *IEEE Transactions on Power Systems*, vol. 30, no. 5, pp. 2726–2735, 2014.

[27] J. Song, E. Cotilla-Sanchez, G. Ghanavati, and P. D. Hines, "Dynamic modeling of cascading failure in power systems," *IEEE Transactions on Power Systems*, vol. 31, no. 3, pp. 2085–2095, 2015.

[28] D.-X. Zhang, D. Zhao, Z.-H. Guan, Y. Wu, M. Chi, and G.-L. Zheng, "Probabilistic analysis of cascade failure dynamics in complex network," *Physica A: Statistical Mechanics and its Applications*, vol. 461, pp. 299–309, 2016.

[29] X. Zhang, C. Zhan, and K. T. Chi, "Modeling the dynamics of cascading failures in power systems," *IEEE Journal on Emerging and Selected Topics in Circuits and Systems*, vol. 7, no. 2, pp. 192–204, 2017.

[30] J. Qi, J. Wang, and K. Sun, "Efficient estimation of component interactions for cascading failure analysis by em algorithm," *IEEE Transactions on Power Systems*, vol. 33, no. 3, pp. 3153–3161, 2017.

[31] M. Jaggi, "Revisiting frank-wolfe: Projection-free sparse convex optimization.," in *ICML (1)*, pp. 427–435, 2013.

[32] "IEEE Power Systems." `https://github.com/MATPOWER/matpower`.

[33] "Newton-Raphson Method." `https://wiki.openelectrical.org/index.php?title=Newton-Raphson_Power_Flow`.